The Pinhole/Occulter Facility

Edited by
E. A. Tandberg-Hanssen
George C. Marshall Space Flight Center
Marshall Space Flight Center, Alabama

H. S. Hudson
University of California
San Diego, California

J. R. Dabbs
George C. Marshall Space Flight Center
Marshall Space Flight Center, Alabama

W. A. Baity
University of California
San Diego, California

NASA-TP-2168 19830017375

The Pinhole/Occulter Facility

25

PINHOLE / OCCULTER
FACILITY

FOURIER-TRANSFORM
GRIDS

CODED APERTURE
PATTERN

VISIBLE / UV
OCCULTING
DISK

ASPECT
REFERENCE
SYSTEM

ULTRAVIOLET
OCCULTING EDGE

OCCULTER
PLANE

50 m

DEPLOYABLE
BOOM

ULTRAVIOLET
CORONAGRAPH-
SPECTROMETER

X-RAY DETECTORS

VISIBLE / UV
CORONAGRAPH

COLLIMATOR
AND WINDOW
STRUCTURE

BOOM CANISTER

ASPECT AND
ALIGNMENT SYSTEM

DETECTOR PLANE

Contents

Table 1.1 Parameters of a Model Pinhole/Occulter Facility

X-ray Observations

Angular resolution	0.2 arc sec
Field of view	1 degree
Total area	15000 cm^2
Time resolution	1 msec
Spectral range	2—120 keV
Sensitivity @ 20 keV	10^{-5} ph/cm^{2}sec keV
Sensitivity @ 5 keV	0.03μJy
Mass	450 kg
Power	250 watts
Telemetry	250 kbps

Coronal Observations

Ultraviolet Coronagraph-Spectrometer

Angular resolution	1 arc sec
Telescope aperture	44 × 44 cm
Time resolution	10 sec
Spectral range	300—1700 Å
Spectral resolution $\lambda/\Delta\lambda$	10000
Sensitivity	5 × 10^5 ph/cm^{2}sec sr
Magnetic sensitivity	< 2 gauss
Deployed Size	1.3 m × 1.3 m × 5.5 m
Mass	280 kg
Power	140 watts
Telemetry	120 kbps

Visible/UV Coronagraph

Angular resolution	1 arc sec
Telescope aperture	50 cm
Time resolution	1 sec
Spectral range	1100 Å—1.1 μ
Spectral resolution	broad-band and line filters
Sensitivity	14th mag. at 3 R$_0$
Size	1 m × 1 m × 2.5 m
Mass	200 kg
Power	130 watts
Telemetry	1 Mbps

Overall System

Boom length (deployed)	50 m
Mass of occulter	50 kg
Total mass	4200 kg
Total volume	1.5 pallets
Power	570 watts
Telemetry	1.4 Mbps

Preface

The outer solar atmosphere exhibits a great variety of dynamic and energetic plasma phenomena, from the catastrophic energy release of solar flares to the steady acceleration of the solar wind. Observations from space during the past two maxima of the solar activity cycle have laid the groundwork for understanding the physics of the solar corona. The Pinhole/Occulter Facility contains the instruments necessary for achieving fuller knowledge: broad-band X-ray imaging, combined with simultaneous ultraviolet spectroscopy and visible/UV imaging.

Recent spectroscopic measurements with a new rocket-borne ultraviolet coronagraph together with white-light observations have demonstrated the feasibility of determining the plasma properties of the extended solar corona. The Pinhole/Occulter Facility will provide the instrumentation required to apply such measurements to detailed studies of the physics of solar wind acceleration and coronal activity. At the same time, X-ray astronomy has progressed, through the surveys by small satellites and the "deep" observations of soft X-rays by the *Einstein* Observatory, to a level at which it has become a major component of astronomical investigation. The Pinhole/Occulter represents the first serious effort to broaden the spectral band available to X-ray astronomers at high angular resolution (below one arc sec), and is an effective complement to AXAF and other future soft X-ray facilities.

The Pinhole/Occulter Facility originated as a concept during the discussions of the NASA Facility Definition Team for Hard X-ray Imaging, formed in response to an Announcement of Opportunity (AO #5) for the development of instrumentation for Spacelab. A full account of the proceedings of this Facility Definition Team is given in the document UCSD-SP-79-03 and in the minutes of its meetings, and in proposals for Spacelab instruments based upon the concept. Following this, an *ad hoc* committee to study the pinhole concept was formed. It was realized at the outset that the long focal length needed for hard X-ray imaging would make advanced coronal observation possible as well; the *ad hoc* committee therefore included representation in this discipline. The report of the *ad hoc* committee (NASA TM-82413, 1981) describes a model configuration of the facility and its instrumentation which largely matches that described below. In response to the activities of this committee, NASA in 1980 formed a Science Working Group for the study of the concept. This group includes X-ray astronomers as well as solar physicists.

The present report summarizes the scientific definition at a pre-phase A level by the Science Working Group for the Pinhole/Occulter Facility. A companion second volume giving further technical details and the results of engineering analysis will appear in Spring 1983. The Pinhole/Occulter concept has now reached the level of scientific and engineering definition at which a full systems analysis in a Phase A study of concept feasibility should be undertaken.

The Science Working Group would like to thank the National Aeronautics and Space Administration for the support and assistance it has received from J. Parker, C. De Sanctis, and many other people at the Marshall Space Flight Center in the course of these studies. The continued support of NASA

The Pinhole/Occulter Facility Science Working Group

R.L. Blake	Los Alamos Scientific Laboratories
C.J. Crannell	NASA Goddard Space Flight Center
J.R. Dabbs (secretary)	NASA Marshall Space Flight Center
E.E. Fenimore	Los Alamos Scientific Laboratories
G.P. Garmire	Pennsylvania State University
M.E. Greene	U. of Alabama, Huntsville
J.E. Grindlay	Center for Astrophysics
H.S. Hudson (co-chairman)	U.C. San Diego
G.J. Hurford	California Institute of Technology
J.L. Kohl	Center for Astrophysics
R.P. Lin	U.C. Berkeley
R.H. Munro	High Altitude Observatory
F.Q. Orrall	Institute of Astronomy, Honolulu
E.A. Tandberg-Hanssen (co-chairman)	NASA Marshall Space Flight Center
H.F. van Beek	Space Research Laboratory Utrecht
A.P. Willmore	U. of Birmingham
K.S. Wood	Naval Research Laboratory

1. Executive Summary

1.1 Introduction and Summary

The Pinhole/Occulter Facility is a novel instrumentation concept that will provide a major improvement in sensitivity and resolution for both X-ray and coronagraphic observations of the nonthermal phenomena central to understanding solar activity. It will also make possible high-energy cosmic X-ray observations with unprecedented angular resolution (0.2 arc sec) and will provide hard X-ray information complementary to the soft X-ray data from AXAF. In essence, the Pinhole/Occulter Facility consists of a long boom, erected from the Shuttle bay or other space platform, separating an X-ray mask/occulting disk from X-ray detectors and coronagraphs. The long separation permits very high angular resolution.

The Pinhole/Occulter is designed to study the nonthermal phenomena that lie at the heart of plasma dynamics in the solar corona. These include the acceleration of nonthermal particles in solar flares and in disturbances of the corona, as well as the expansion of the corona into interplanetary space to form the solar wind. The Pinhole/Occulter will provide key information regarding the energetics of solar flares, with diagnostic information that can relate flare phenomena to the powerful acceleration of 10−200 keV electrons in the energy-release phase. The corona, as revealed by observation over the last solar cycle, consists of a tangled network of complex elements organized by electrodynamic processes. In and among the magnetic structures, the plasma exhibits a wide range of physical parameters. The interactions among these elements — and with the transition region which links the active corona with the chromosphere — produce the phenomena of solar activity and the solar wind. Diagnostic information on all spatial and temporal scales, including the smallest, is essential for an accurate description of these phenomena.

The Pinhole/Occulter also will provide a facility for X-ray astronomy that combines broad spectral response, excellent angular resolution, and high throughput into a large-area detector (1.5 m²). Such an instrument will fruitfully observe a wide range of astronomical sources, ranging from extragalactic (active galaxies and clusters) to galactic (supernovae, obscured objects such as the galactic center, and stars). The stellar observations deserve particular mention because in many cases they involve similar physics to that of the solar observations.

Some of the important scientific questions addressed by the Pinhole/Occulter are:

What are the mechanisms of particle acceleration at the Sun, in flares and in the corona?

What is the nature of energy release in solar flares?

What mechanisms provide the energy and momentum for the solar wind?

What propels coronal transients and flare ejecta?

How do active galactic nuclei couple with their environments?

What are the mechanisms of particle acceleration and propagation within supernova remnants?

What are the physical conditions in the acceleration regions of jets?

The instrumentation necessary to confront these questions must provide a long baseline — 50 meters in the model configuration — separating the occulter from the detector-plane instruments. For X-ray observations, this long baseline permits the high angular resolution of 0.2 arc sec to be reached. For coronal observations in the visible/UV and out to the extreme ultraviolet, the occulter provides a large shadow — similar to a total eclipse of the sun — allowing large-diameter optics to achieve high angular resolution and great sensitivity. High sensitivity also makes possible the high spectral resolution with which the physical parameters in the distant corona can be probed. For both X-radiation and for classical coronal observations, the Pinhole/Occulter technique provides *qualitatively* new observational capability. In the next cycle of solar activity we therefore anticipate an even greater gain in knowledge than has been achieved in the past one.

1.2 Scientific Background

The solar corona represents a frontier for solar astrophysics: it is faint, so observations have been difficult, and it contains many puzzles and problems not answered by traditional astronomical theories. We know that the solar wind blows, but not how it obtains its mass

and energy from the cooler layers of the atmosphere. We know many effects of transient phenomena in the corona — including some felt on the surface of the Earth — but know little of the causes or mechanisms involved. We know that there is an intimate involvement of the corona with solar flares and with other manifestations of solar activity, but we do not understand the plasma physics well enough to know how the energy is stored and released into spectacular forms. In the most striking energy release, the flare, we have not been able to trace the energy release in the impulsive phase from source to sink.

The image of the corona in Figure 1.1 shows fine structure at the resolution limit of the observations. *The physics of the solar corona depends upon the properties of this unresolved substructure in ways that are not understood.* The exploration of the physics of these structures is the main goal of the Pinhole/Occulter Facility. The answers will explain energy transfer and deposition, the acceleration of energetic particles and of the solar wind itself, and the motion of the transients through the coronal structures.
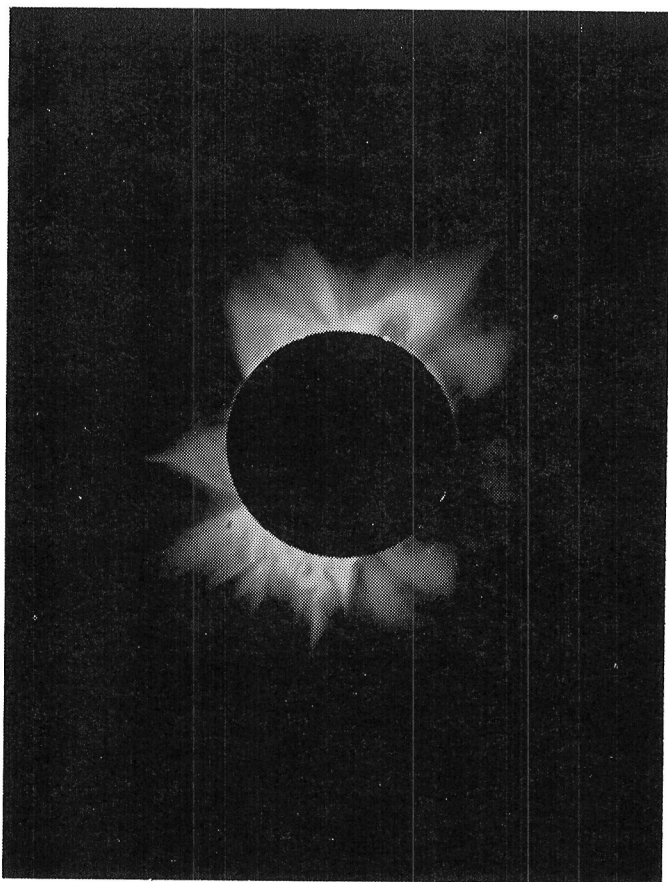

Figure 1.1—Solar corona: the solar eclipse of 1980 Feb 16, photographed at Pelem, India (Courtesy High Altitude Observatory and Southwestern at Memphis).

Coronal physics has depended upon four major observational windows: white light, emission lines from the lowest corona in wavelengths down to the soft X-ray region, radio frequencies, and the *in situ* measurements possible in the solar wind. Adequate *diagnostic* information is not presently available — even on coarse angular scales — in vital spectral regions. The Pinhole/Occulter Facility will give the first detailed hard X-ray observations and will permit emission-line diagnostics throughout the corona, significantly expanding our diagnostic and remote-sensing knowledge of the dynamic coronal plasma.

X-ray observations of the corona have much scientific matter in common with galactic and extragalactic X-ray astronomy. For example, the acceleration and transport of nonthermal electrons are important processes that have not been studied adequately in supernova remnants, galactic nuclei (including our own), and clusters of galaxies. The Pinhole/Occulter Facility will greatly extend the spectral range over which these objects can be studied; more importantly, it will provide higher angular resolution than that which has been available to date.

1.3 Scientific Objectives

The scientific objectives of the Pinhole/Occulter Facility can be divided into four major areas: solar activity, coronal structure and solar-wind generation, coronal transients, and X-ray astronomy. The nonsolar observations use the same instrumentation, and many of the specific scientific problems are related to the solar ones. In the following we detail the primary scientific objectives.

1.3.1 Solar Activity

X-radiation is the natural emission medium for the bulk of the solar corona. The corona consists of million-degree plasmas interacting dynamically, with occasional intrusions of relatively cold matter. The plasmas are quite active, and the techniques of radio astronomy show that innumerable plasma instabilities, particle accelerations, and other essentially *nonthermal* phenomena characterize this activity. The observations of the corona to date have only partly explored its complexities, and vital observations (including those described briefly below) have not yet been possible.

The solar X-ray observations of the Pinhole/Occulter Facility will provide an angular resolution limited by diffraction at 0.2 arc sec. This angular resolution equals approximately the angle subtended by the density scale height in the coolest part of the solar atmosphere,

a shortest characteristic distance scale of ~ 150 km. At the same time the use of large-area detectors will give unprecedented sensitivity for the study of faint coronal sources. Given these capabilities, two major observational areas are opened up: the study of particle acceleration in solar flares, especially the relationships among nonthermal and thermal phenomena in the lower corona, transition region, and chromosphere; and the study of coronal phenomena directly in the bremsstrahlung of freshly accelerated electrons.

Solar flares consist of at least two distinguishable phases of energy release: *impulsive* and *gradual*. The impulsive phase produces the striking microwave and hard X-ray bursts that show the presence of the intense acceleration of 10—100 keV electrons. Gamma-ray observations indicate that acceleration of ions to relativistic energies also occurs in the impulsive phase. Electrons accelerated during the impulsive phase often contain a large fraction (up to 10^{32} ergs greater than 20 keV) of the total flare energy. The most urgent problem in understanding this energy release lies in determining precisely where it occurs within the large-scale structure of the flare. Hard X-ray imaging observations from the Solar Maximum Mission have detected in a few large flares the high density footpoint regions where the accelerated electrons lose most of their energy. In contrast, high resolution microwave mapping of the same flares shows brightening at the tops of the magnetic loops, in between the footpoints (Figure 1.2).

The Pinhole/Occulter Facility will provide the orders of magnitude increase in sensitivity and in angular and temporal resolution needed to locate the *acceleration/flare energy release* region, which is believed to be in the low density corona, and to trace the propagation of the energetic electrons through the flare structure. Then complementary soft X-ray, EUV and optical observations can provide diagnostic information to help answer these fundamental questions:

— *Where does the particle acceleration and energy release occur in flares?*

— *What are the mechanisms which accelerate particles in solar flares?*

— *What is the nature of the energy release in solar flares?*

Figure 1.2—The hard X-ray sources (squares representing bright 8 arc sec pixels as observed from the Solar Maximum Mission) lie at opposite foot points of a magnetic flux tube. The microwave contours, from VLA observations, show the top of the tube (Hurford, 1982).

In addition, the P/OF X-ray measurements will delineate the role of the energetic particles in other flare phenomena such as the production of EUV, white light and other impulsive phase emissions; the evaporation of new material into the corona to form the high temperature flare plasmas; and the ejection of material from the Sun with the formation of shock waves.

1.3.2 Coronal Structure and Solar-Wind Generation

Observations of the solar corona from space have reached a technological plateau in the exploitation of relatively small apertures in visible light. Future developments will emphasize spectroscopic observations over a broad range of wavelengths, large-aperture optics, and resonance-line diagnostic studies of the physical conditions in the solar-wind acceleration region of the corona. We have identified several specific problems:

What mechanisms deposit energy and momentum in the corona? The generation of the solar wind on open field lines and the heating of the solar corona in closed magnetic structures (especially in active regions) are two very significant unsolved problems. The Pinhole/Occulter observations will provide the necessary diagnostic information to study the physical processes of energy and momentum transfer on angular scales small enough to resolve the relevant structure.

How do the physical properties of coronal magnetic loops depend upon their photospheric origin? As seen in Figure 1.3, both active and quiet regions of the sun contain elaborate networks of loops that link the photosphere with the corona. Such loops may connect different active regions or even different hemispheres. The Pinhole/Occulter observations will provide diagnostic information on these structures and the transition between open and closed magnetic field regions of the coronal plasma.
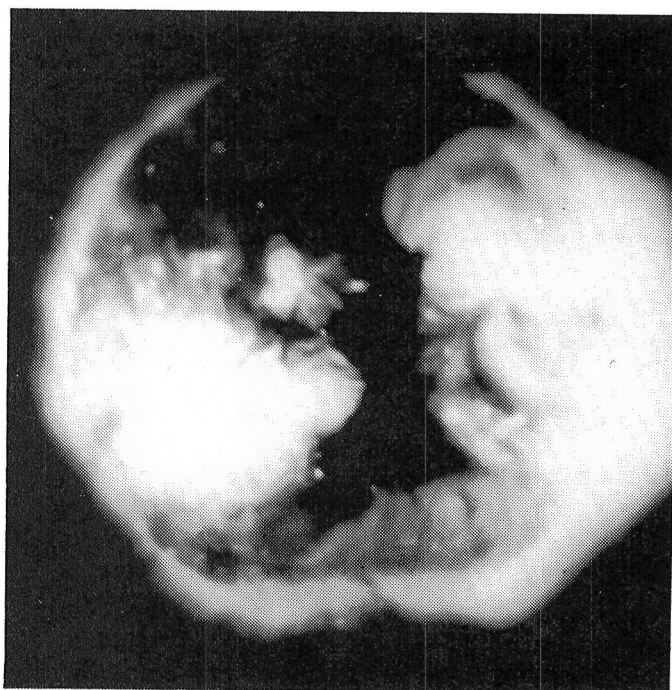

Figure 1.3—Skylab image of soft X-ray corona (courtesy American Science and Engineering).

1.3.3 Coronal Activity

The corona exhibits stable structures, but it also contains many types of variations and transient phenomena. The intense and highly organized radio emission shows that *nonthermal* processes accelerate particles to high energies during various types of transient perturbation. The plasma physics of these unstable regions is generally known only sketchily, since virtually no direct diagnostic observations exist. The active corona represents a true frontier for solar physics, with broad implications for many other astrophysical and laboratory investigations.

What propels coronal transients? The expulsion of a coronal transient requires a great deal of energy. For the flare-related transient, the energy in the coronal disturbance may exceed that in the other known forms of flare energy release. The source of this energy is presently unknown; the participation of the corona itself in stabilizing or energizing the material that forms the transient is not understood. The Pinhole/Occulter Facility will let us make diagnostic observations in the magnetic structure of these transients.

How are nonthermal particles accelerated in the corona? Each of the numerous types of radio bursts known at meter wavelengths requires a different population of nonthermal electrons. The mapping of source regions in hard X-radiation, together with diagnostic information from the P/OF coronal instruments, will show us where and how the particle accelerators work.

1.3.4 X-ray Astronomy

The observational goals of X-ray astronomy match closely those desired for the solar corona: high sensitivity, high angular resolution, high time resolution, and broad spectral coverage. The Pinhole/Occulter is thus a general-purpose instrument suitable for a broad variety of objectives in X-ray astronomy. Specific targets for observation range from solar-type phenomena in stars to exotic objects such as neutron stars and black holes. For extended objects, including clusters of point sources, the Pinhole/Occulter will provide detailed images with unprecedented angular resolution.

How do active galactic nuclei interact with their environments? X-radiation provides a tool for observing high-energy particles in the nuclei and jets found in active galaxies. The VLBI radio observations of these objects show that they contain angular structure on a wide variety of angular scales. The X-ray and radio observations are complementary probes of the distributions of matter and fields in the sources; the objective of the Pinhole/Occulter observations will be to discover the energetics and mechanisms of the jets. Figure 1.4 shows the *Einstein* image of the giant radio galaxy Cen A, indicating the existence of a barely resolved X-ray lobe structure oriented with the radio and optical jets. Response in the hard X-ray band will permit the Pinhole/Occulter to probe further into the acceleration regions of both galactic and extragalactic jets.

How do nonthermal particles propagate in supernova remnants? Supernova remnants may accelerate high-energy particles, perhaps by mechanisms resembling those found in the solar corona. The most spectacular

example is the Crab Nebula (Fig. 1.5), in which the pulsar is directly responsible for particle acceleration. Pinhole/Occulter observations will reveal the details — at very high resolution — of the propagation of energetic electrons in the wisps and filaments.
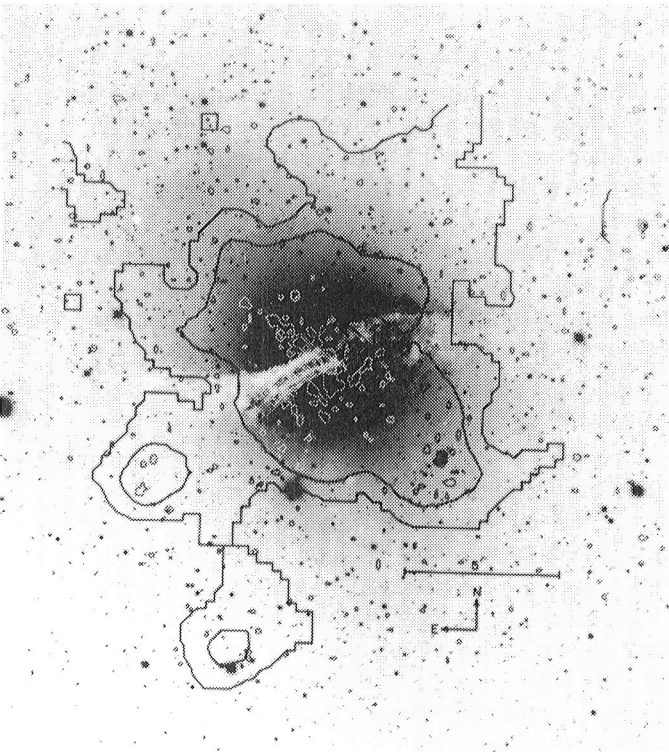

Figure 1.4—Superposed optical and X-ray (Einstein) images of the nearby radio galaxy Cen A. Black contours show Einstein data with arc-minute resolution; white contours (high resolution X-ray data) show the jet emerging from the nucleus of the galaxy (Feigelson *et al.*, 1982).

1.4 Scientific Requirements

The problems discussed above require for their solution a new order of high-resolution, high-sensitivity observations of X-radiation and of coronal visible and ultraviolet emissions. The X-ray observations should have sub-arc sec resolution to match the resolution available now or in the near future in other wavelength bands. The sensitivity of the X-ray observations must be very high in order to detect the faint hard X-ray emissions from the solar corona. This implies a large collecting area. Finally the use of large-aperture coronal telescopes is also mandatory both to achieve fine spatial resolution and to obtain the high sensitivity and good time resolution resulting from high photon counting rates.

The direct solution to these requirements is the creation of a facility capable of maintaining a large separation, on the order of 50 m, between an occulter and the various telescopes and detectors. The relationship between the diffraction-limited angular resolution Θ in arc sec, the boom length l in m., and the lowest available energy E in keV, is given by $\Theta^2 \, l / E = 50$. For X-ray observations the simplest kind of imaging system that can take advantage of the long separation to produce high resolution is the pinhole camera: a small hole in the remote occulter will produce a sharp image on the detector array. Practical versions of such an imager use multiple holes in an optimum coded-aperture array to give a high throughput.

The remote occulter will also provide a large shadow area at the detector plane. Large-aperture optics (diameters of order 50 cm) can then make sensitive observations of the faint solar corona with good time resolution. The large aperture will also result in excellent diffraction-limited spatial resolution.

A concept for the Pinhole/Occulter Facility that makes use of the resources of the Space Transportation System is described below briefly, and illustrated in the frontispiece.
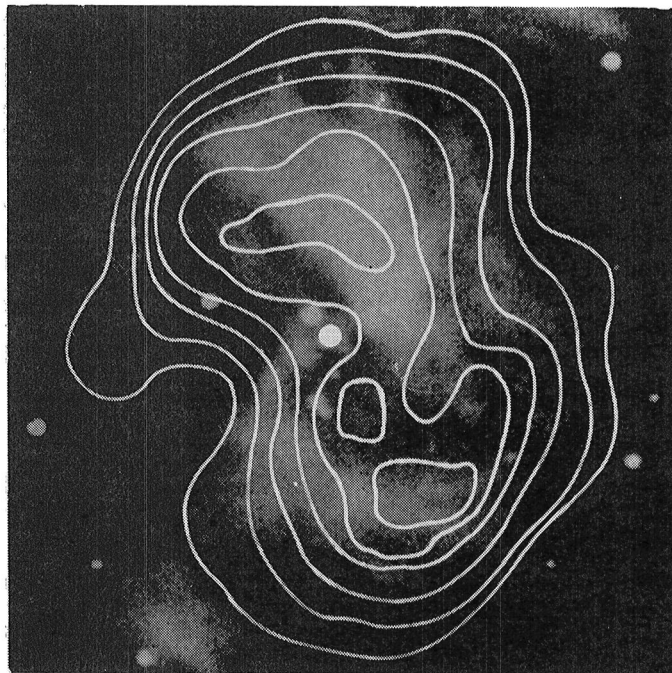

Figure 1.5—Soft X-ray (Einstein) and hard X-ray images of the Crab Nebula, the latter (contour lines) from balloon observations (Makishima and Pelling, 1982).

1.5 Configuration Concept

The Pinhole/Occulter Facility consists of a self-deployed boom of 50 m length, which separates an *occulter plane* from a *detector plane*. The X-ray detectors and coronagraphic optics mounted on the detector plane are analogous to the focal-plane instrumentation of an ordinary telescope, except that they use the occulter only for providing a shadow pattern. The occulter plane is passive and has no electrical interface with the rest of the Facility. The standard Instrument Pointing Subsystem orients the boom to within a few arc sec of the point observed. The general layout is as shown in the frontispiece of this report. Table 1.1 gives general information about the Pinhole/Occulter Facility, together with the observational characteristics of the model detector-plane instruments.

1.5.1 Facility

The facility consists of the occulter plane, the retractable boom, the detector plane, and the alignment system. The boom is of a type used for deployment of spacecraft antennas and solar panels. Booms of comparable dimensions have been built and tested. The control of the boom requires active control of the lowest frequency resonant modes. The technology exists and can be tailored to the Pinhole/Occulter application, as shown by detailed modeling of the boom dynamics in the Shuttle mechanical environment.

Accurate aspect sensing and the internal transfer of the information is an important element of the Pinhole/Occulter system, because the desired angular resolution is comparable to that of the best at any other wavelength except for VLBI radio astronomy. The availability of aspect-sensing technology for the 0.2 arc sec resolution of the Pinhole/Occulter depends strongly upon progress in other programs. The Space Telescope, SOT, AXAF, or other high-resolution Spacelab experiments will establish the necessary technology within the time frame appropriate for the Pinhole/Occulter.

1.5.2 X-ray Instrumentation

There are two imaging X-ray systems: a *high-resolution imager*, with an angular resolution of 0.2 arc sec, and a *high-sensitivity imager*, with a large field of view and a total detector area of 1.2 m². The high-resolution imager uses Fourier-transform X-ray optics, a modern derivative of the modulation collimator,

requiring one grid on the occulter plane and one at the detector itself. The detector is mounted on an x-y stage so that the 3.4 arc minute field of view can frame a suitable solar active region. The high-sensitivity imager is a straightforward coded-aperture system, with a single grid on the occulter plane and a large (> 1°) field of view. Section 1.6 explains these techniques further.

The two X-ray detection systems have been designed to bring X-ray observational capability to a level matching that of the best optical (SOT) and microwave (VLA) facilities. The coronal hard X-ray observations of the Pinhole/Occulter will have substantially higher resolution (8 arc sec) than coronal observations at meter wavelengths (generally ~ 1 arc min), our best guide heretofore on the nonthermal effects in the dynamic corona.

The total area (1.5 m² in five 3000 cm² modules) of the Pinhole/Occulter X-ray detectors makes it comparable to the largest X-ray astronomy counter experiments. In addition to the resulting high sensitivity, the coded aperture provides very good angular resolution. An integration of 10^4 sec for an energy band of 2—10 keV would detect (5σ) a point source at 30 nJy (0.03 UFU). The counters themselves are xenon-filled position-sensitive multiwire proportional counters, based upon the technology established by HEAO-1.

1.5.3 Coronagraphic Instrumentation

Two separate telescopes on the detector plane use the occulter for sensitive visible light and ultraviolet coronal observations. These instruments are not coronagraphs of the types previously used for observations from space; they exploit the large-diameter shadow in a manner more nearly resembling eclipse observations. The visible light/UV telescope has optics of 50-cm diameter, while the telescope of the ultraviolet coronagraph-spectrometer has a 44-cm aperture. The latter instrument obtains spectroscopic information in the 300—1700 Å spectral range with a resolution of $\frac{\lambda}{\Delta\lambda}$ = 1 × 10⁴. Stray-light suppression requires an internal occulter as well as the use of vignetting by the remote occulter. The visible/UV instruments obtain coronal images in broad band white light and at selected visible and UV wavelengths. Each coronal telescope has an angular resolution of 1 arc sec and is capable of imaging a 90° sector of the corona out to 10 R_0 from the sun's center.

1.6 Hard X-ray Imaging

At X-ray energies above about 10 keV, focusing optics become very inefficient because of the difficulty of obtaining refraction or reflection. The formation of images at higher energies relies upon making shadow patterns with the incident radiation, an approach that began with the·invention of the modulation collimator (Oda 1965) and which has had numerous applications in X-ray astronomy (Bradt et al. 1968; Oda 1982).

For solar observations, the Hard X-ray Imaging Spectrometer (HXIS) on the Solar Maximum Mission is the most sophisticated hard X-ray imaging system yet flown (van Beek et al. 1980). It produces a direct image with resolution of 8 arc sec (FWHM) through the use of multiple grids and a very rigid and precise metering structure. The sensitivity of such a collimator is quite low, because each detector element is dedicated to viewing only a single area on the sun. Because of this and the difficult mechanical problems represented by the metering structure and the alignment of the multiple grids, it is clear that this approach cannot easily be extended to produce a breakthrough in resolution and sensitivity.

In the years since the HXIS experiment was defined, high-resolution imaging with major gains in sensitivity has become possible with techniques that do not require precise metering structures. In particular, considerable progress has been made in coded-aperture imaging (Dicke 1968), where a single mask containing multiple pinholes produces many overlapping simple images on a position-sensitive detector (Figure 1.6). A single image may then be produced by a straightforward correlation function. This type of imaging system has a multiplex advantage to provide very high sensitivity, since fully half of the detector area can observe all regions of the source. Furthermore, such a single-grid approach avoids the need for a precise metering structure. The modern developments such as the "uniformly redundant array" (Fenimore and Cannon 1978) have excellent image quality (Figure 1.7). For a given mask-detector separation, the angular resolution is limited by the spatial resolution of the detector; for a 50-meter separation and 1 mm position resolution, one can obtain an angular resolution of 8 arc seconds.

To attain higher resolution, the limitations imposed by the detector characteristics can be overcome by Fourier-transform imaging systems (Makishima et al. 1978). This technique requires a pair of grids, which are divided into a moderate number of separate areas called subcollimators. Each of the $\sim$10-100 subcollimator grids has a set of slits with a distinct orientation and width (Figure 1.8). The illumination pattern for each subcollimator, as measured by a detector with only moderate spatial resolution, can be shown to represent a single Fourier component of the spatial distribution of the X-ray source (Hurford and Hudson 1982). In precise mathematical analogy to aperture synthesis in radio astronomy, the set of subcollimator outputs can then be Fourier-transformed to yield an image of the source (e.g. Fomalont and Wright 1974) using the data-processing techniques that have been highly developed for radio telescopes such as the Very Large Array (VLA).
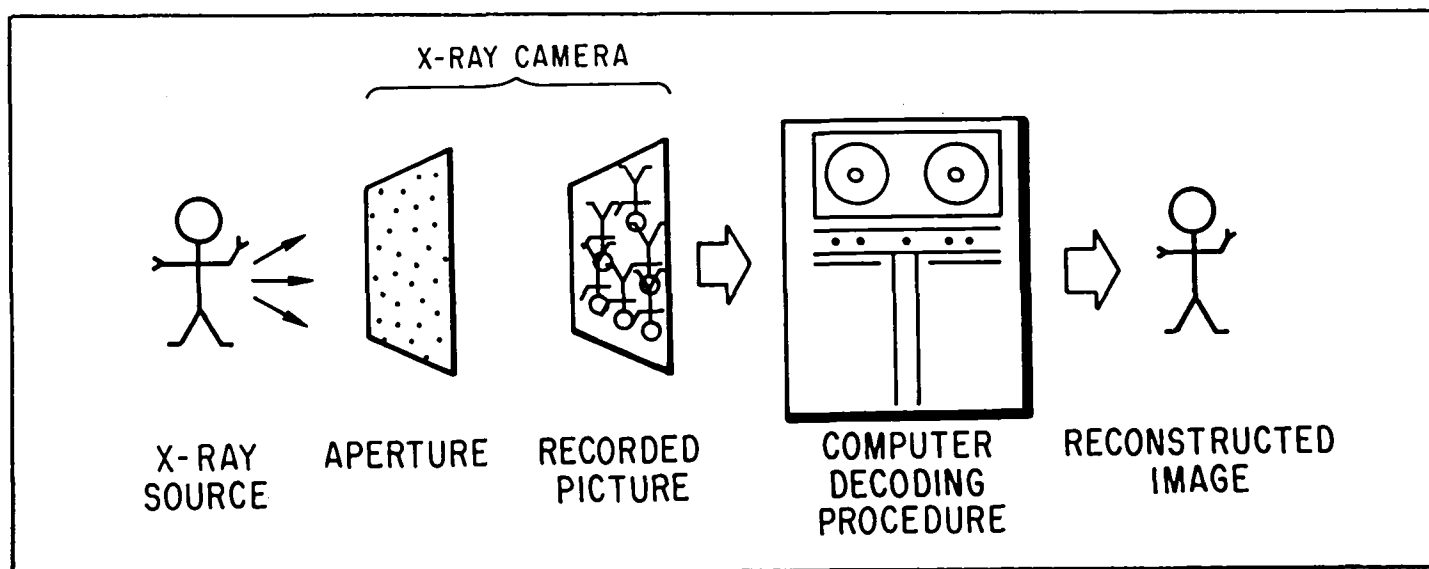

Figure 1.6—The basic steps in coded aperture imaging. The aperture consists of many holes. Thus, many overlapping images of the source are observed simultaneously, but have to be de-multiplexed or decoded. The special distribution of holes (i.e., a uniformly redundant array) allows the unfolding to be performed without the introduction of artifacts (Fenimore et al., 1979).

Although this approach requires two sets of grids, the Fourier-transform system requires precise knowledge only of their relative displacement; control of their relative placement or orientation does not need to be very precise. The Fourier-transform approach has the multiplex advantage also, and provides almost as much sensitivity as the coded-aperture approach. The coded-aperture imager has better image quality on complex sources and a larger field of view; the Fourier-transform imager has higher resolution. For a 50-m separation and slits 50 microns wide (similar to those of HXIS), a Fourier-transform imager can give 0.2 arc sec resolution.

The Pinhole/Occulter Facility requires the use of both types of imaging system in order to meet the scientific objectives for the X-ray observations. Detailed numerical simulations of the performance of the two types of imaging system have been carried out, leading to the preliminary configuration represented by the model instrumentation described in this report.
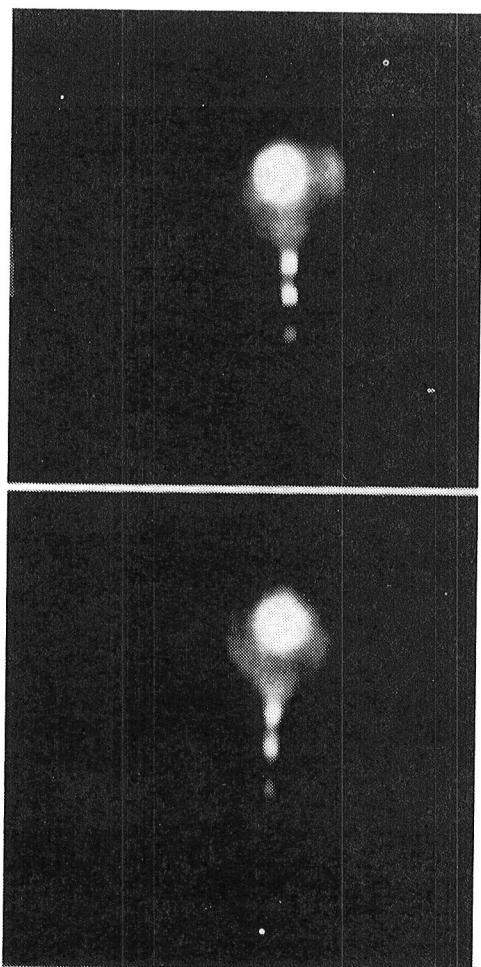

Figure 1.7—A demonstration of the imaging capabilities of coded aperture imaging. Both images are of an implosion of a glass microballoon, seen from different angles during a laser-fusion experiment. The top image is from a conventional pinhole camera and the bottom image is from a uniformly redundant array. The images agree down to the level of detectable features (1% of peak). Differences (such as in the halo) are due to the different look angles. Seen are the bright core, which is the compressed, laser-heated DT fuel; the halo, which is the remains of the glass microballoon; and bright points on the supporting stalk (Fenimore *et al.*, 1979).

Figure 1.8—Schematic views (not to scale) of a Fourier transform X-ray telescope. The top panel shows two widely separated grids, each of which is divided into several subcollimators. Because of a slight difference in the spacing of the top and bottom slits in each subcollimator, the spatial distribution of counts (lower panel) measures a Fourier component of the source. The choice of Fourier component is determined by the width and orientation of the slits. As in radio interferometry, measurements of many Fourier components can be transformed to yield an image of the source (Hurford and Hudson, 1982).

1.7 Facility Development

This document constitutes Volume I of the Final Report of the Pinhole/Occulter Facility Science Working Group; the remainder of the report details the scientific definition of the P/OF observational program, together with the instrumental requirements for these observations. The second volume of the Final Report is to be released in Spring 1983, and will contain the results of technical and feasibility studies as well as a more detailed account of the instrument concept. The two volumes together comprise a pre-phase A definition of the Pinhole/Occulter Facility. The next programmatic step in the development should consist of a Phase A study, which will provide a detailed feasibility assessment within the resources of the Space Shuttle and its capabilities for supporting such scientific investigations. The Phase A study will also provide a basis for realistic cost estimates based upon a hardware development plan.

The Pinhole/Occulter Facility is a stand-alone Shuttle facility suitable for advanced studies of solar flares, the solar corona, and cosmic X-ray sources. In these areas the brief exposure of a sortie mission will generate an excellent scientific return, and the versatility of the Shuttle should make possible several flights oriented to specific astrophysical questions. Ultimately, however, the Pinhole/ Occulter should become a part of a longer-term space observatory. There are three essential reasons for this: observations of rare transient phenomena are needed; longer-term synoptic coverage is essential for understanding and monitoring other phenomena, including the generation of the solar wind; and long exposure times are required for certain faint sources.

The optimum step in the evolution of the Pinhole/ Occulter Facility therefore appears to be the creation of an advanced, comprehensive observatory on a semi-permanent platform in space. For solar observations this would be the Advanced Solar Observatory, incorporating the Solar Optical Telescope along with advanced instrumentation in other wavelength regions. The Solar Maximum Mission has shown clearly that a coordinated group of telescopes and detectors offers many advantages in probing the strongly inhomogeneous and time-varying phenomena found in the solar atmosphere. The construction of an Advanced Solar Observatory consisting of state-of-the-art solar instruments would represent an ideal exploitation of the flexibility inherent in the Space Shuttle systems.

For X-ray astronomy the Pinhole/Occulter would evolve differently. Improvements and augmentation of the detectors could proceed until a very large area X-ray observatory came into being. Again a space platform offering long exposure times would be an ideal location for such an evolved Pinhole/Occulter dedicated to X-ray astronomy.

2. Solar X-Ray Observations

The X-radiation from a solar flare results from direct thermal emission of high-temperature plasmas, or from the bremsstrahlung of energetic electrons. The sudden appearance of material at temperatures exceeding 10^7K now appears to be the central act of a solar flare, while the chromospheric (Hα) flare and other low-temperature phenomena are more in the nature of consequences, albeit interesting and important ones. The bulk of the soft X-ray source in a solar flare first appears in the *impulsive phase*, marked by intense bursts of hard X-rays, EUV emission lines, and microwaves. Sensitive and high-resolution observations of soft and hard X-radiation offer us the best opportunity to study the plasma physics of this energy release.

The Pinhole/Occulter Facility has the major observational objective of *defining the geometry of energy release* on sub-arcsecond angular scales. P/OF will provide X-ray observations with sufficient angular resolution to match the optical and radio data from the Solar Optical Telescope (SOT) and the Very Large Array (VLA) to give a comprehensive view of solar activity on angular scales sufficient to isolate nearly homogeneous regions in the solar atmosphere. The sections below describe the scientific areas of interest for the high-resolution X-ray observations. These areas include the *impulsive energy release* of solar flares, as marked by intense hard X-ray and microwave emission; the *gradual energy release* into hot, dense loops; and the *coronal nonthermal activity* that may occur with or without a solar flare. Section 4 of this report emphasizes coronal phenomena observable with both the X-ray and coronagraphic instruments of P/OF.

2.1 Flare Impulsive Phase

Intense hard X-ray and microwave bursts mark the impulsive phase of a solar flare, as illustrated in Figure 2.1. To produce the fluxes observed, a substantial fraction of the total flare energy must go into the acceleration of 10—100 keV electrons during this phase, with the collisional energy losses of these electrons subsequently contributing to other phenomena observed in flares.

The geometry of the impulsive phase appears to consist of closed magnetic flux tubes, since we know from interplanetary observations that most of the electrons are trapped at the sun (Lin and Hudson, 1971; 1976). The observations from the Solar Maximum Mission and *Hinotori*, plus the stereoscopic observations

(Kane *et al.*, 1982), show that the foot-points of these loops are relatively bright hard X-ray sources. These bright footpoints are probably produced by electrons which have been accelerated higher up and precipitated into the dense chromosphere; the actual acceleration region would be too faint to have been observed by the instruments used at present. The observations to date have not had sufficient angular resolution to determine whether individual macroscopic flux tubes or filamentary structures are responsible; nor have they clarified the relationship of the impulsive phase to the growth of the hot flare loops that constitute the gradual phase.
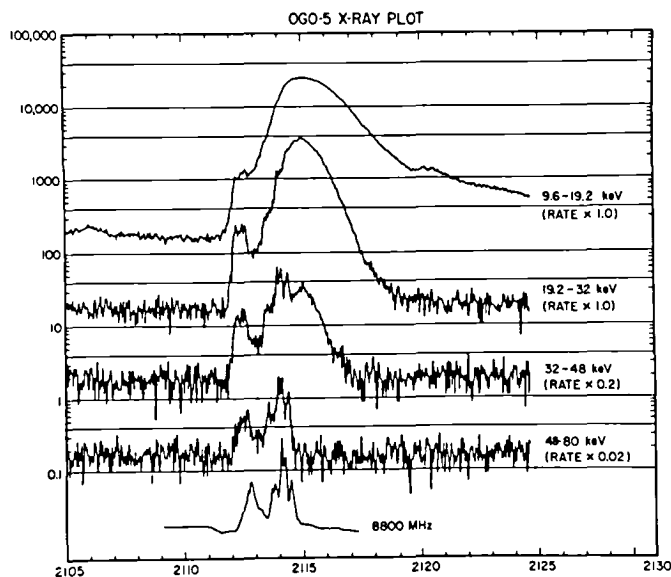
Figure 2.1—The impulsive phase of a solar flare, showing the great similarity between the hard (>50 keV) X-rays and the 8.8 GHz Microwave bursts. The great rounded peak at lower energies is due to high temperature flare plasmas.

HXIS observed numerous flares in its hard X-ray energy bands (16-22 keV and 22-30 keV) that display the characteristic impulsive behavior associated with nonthermal energy release. These hard X-ray sources are compact — often apparently unresolved at 8 arc sec resolution — and appear to be imbedded in the corresponding soft X-ray source. This finding agrees with the reasonable supposition that the hard X-ray emission occurs in the compact magnetic loop structures that start to become visible in soft X-radiation during the impulsive phase energy release.

Further than this, the *foot-points* of the loops appear to be brighter than the tops of the loops. This behavior appeared in at least three flares, those of 1980 April 10 (Hoyng *et al.*, 1981a), 1980 May 21 (Hoyng *et al.*, 1981b), and 1980 Nov. 5 (Duijveman *et al.*, 1982,

which also summarizes the other "footpoint flares"). This evidence for the thick-target interactions of a stream of nonthermal electrons has been corroborated by EUV emission-line observations from SMM (Cheng et al., 1981) which also show foot-point brightenings. Figure 2.2 shows the bright footpoints in the 1980 Nov. 5 flare.
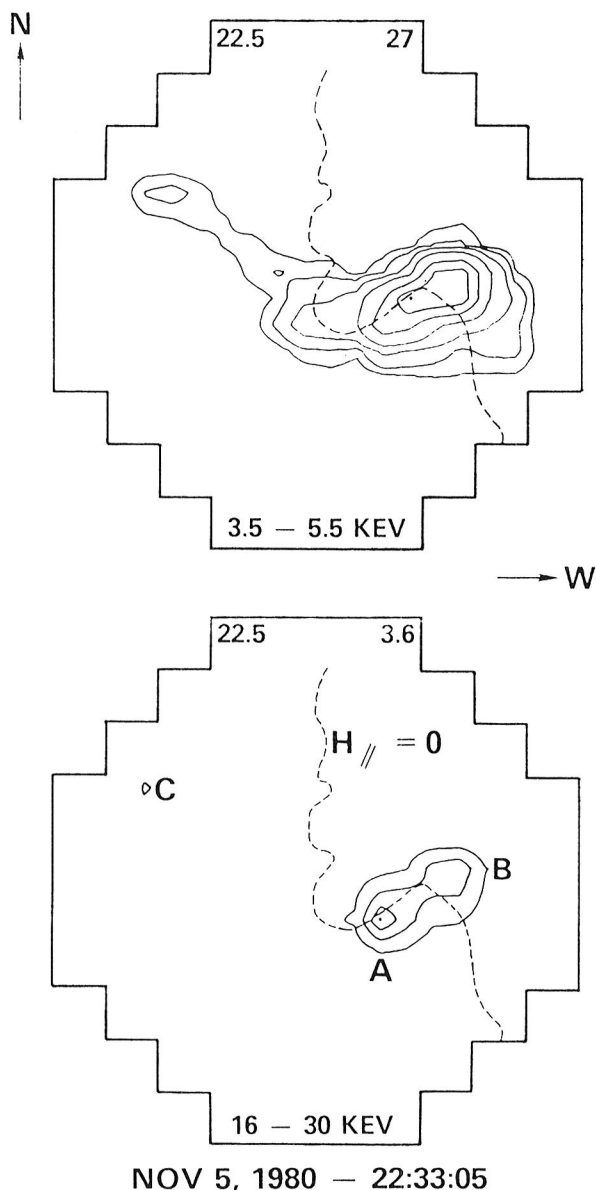
The *Hinotori* observations confirm the tendency of impulsive-phase hard X-ray sources to show a patchy spatial distribution, with evidence that the bright patches occur at the footpoints of coronal magnetic loops. The illustration in Figure 2.3 shows a *Hinotori* observation in which the hard X-ray brightenings matched the Hα ribbon locations quite well (Ohki et al., 1982).

The P/OF X-ray observations will provide sufficient resolution and sensitivity to locate the acceleration and flare energy-release region so that its properties can be studied in detail. For the first time, it will be possible to provide detailed information on the fundamental flare energy release and particle acceleration processes. While the SMM and *Hinotori* X-ray observations were limited to a resolution of ~ 10 arc sec, structure on size scales down to a few hundred km (< 1 arc sec) is known to dominate some solar magnetic phenomena.

NOV 5, 1980 — 22:33:05

Figure 2.2—Contour plots in soft (3.5—5.5 keV) and hard (16—30 keV) X-rays. The frames outline the HXIS fine field of view. The integration time is 22.5 sec during the impulsive spike of the flare of 1980 November 5. The contour levels are 100%, 75%, 50%, 25%, 12.5%, 6.25% and 3.125%. The pixel size is 8" x 8"; corresponding to half the width of one step of the "staircase" shapes at the corners of the fields of view. The hard X-ray bright spots are labelled A, B and C, and the soft X-ray sources can be seen to link these spots. The dashed line shows the magnetic neutral line (Duijveman et al., 1982).
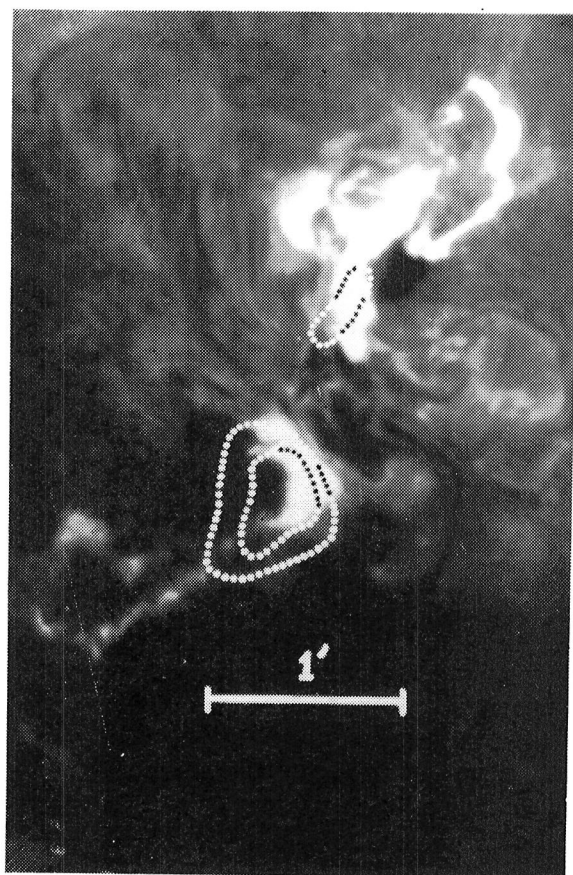

Figure 2.3—Hard X-ray image of the impulsive phase of a flare of May 8, 1981, superposed on an Hα photo image observed at the Big Bear Observatory. The contour levels correspond to 40% and 70% of the peak of the main source.

The ability of P/OF to attain high time resolution at its angular-resolution limit is extremely important. Energy transport even at electron speeds of a few tenths of the speed of light will then become detectable. Motion of a conduction front (Brown *et al.*, 1979) or a wave of "evaporated" chromospheric material at about the ion sound speed would give an X-ray source that drifts more slowly, a few arc sec in a few seconds of time. The detection of such motions will greatly clarify the dynamics of flare phenomena that low-resolution observations have only suggested. Kane and Raoult (1981) have argued that the acceleration site in the impulsive phase may move downward as a flare progresses. Imaging observations will resolve any such motion unambiguously.

2.2 Impulsive Optical/EUV Emissions

The impulsive phase is accompanied by optical and EUV emissions that arise in the transition region and chromosphere, and in rare cases the photosphere also is affected (white-light flares; see the example in Figure 2.2). The white-light continuum was observed in the "first" solar flare (Carrington, 1859), and in a handful of flares since this time (e.g. Svestka, 1976). Related impulsive emissions appear in the extreme ultraviolet, and studies of ionospheric disturbances have shown that an excellent correlation exists between hard X-ray and impulsive EUV emissions (Kane and Donnelly, 1971; Donnelly and Kane, 1979). The impulsive radiation from a solar flare probably represents the deepest atmospheric penetration of the flare phenomenon, resulting from the most intense energy release within the flare area.
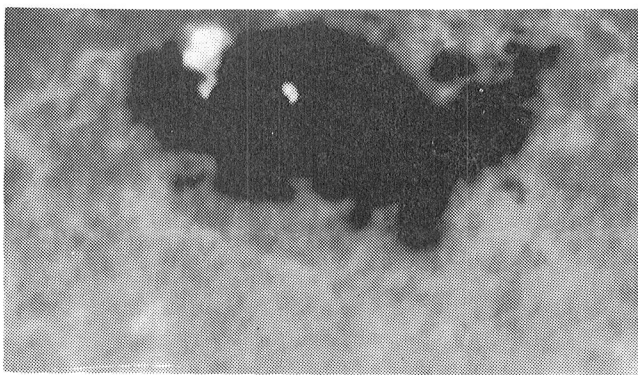

Figure 2.4— White light flare of 24 April 1981, 1357 UT, photographed at 3610 Å (22 Å band). The photo is 200 arc sec wide. Sacramento Peak Observatory photo provided by D. Neidig. The photo is 200 arc sec wide.

The Hα emission of a solar flare — almost the definitive feature of the whole complex of phenomena — is the best-studied chromospheric effect, and recently Acton *et al.* (1982) have shown directly that impulsive Hα brightening coincides with the evaporation of the chromospheric material into the corona. The soft X-ray spectroscopic observations show the heated chromospheric material welling upward during the impulsive phase (Feldman *et al.*, 1981; Antonucci *et al.*, 1982). What is the mechanism of this evaporation? Do nonthermal effects accompany the expansion of flare ribbons in the late phase? These questions require hard X-ray observations with high resolution and good sensitivity.

The mechanisms by which the flare effects reach into the dense atmosphere are not presently known. Candidate theories consider heating by nonthermal particles, by Alfven waves, by compression, or by electrodynamic coupling. The hard X-ray spatial signature of these will generally differ, and the P/OF high-resolution observations have an excellent chance to distinguish among these possibilities by measurements of the strength and location of the heating.

2.3 Two-ribbon Flares

Solar flares viewed in Hα generally tend towards one of two morphologies: compact and two-ribbon (e.g. Sturrock, 1980). The "two-ribbon" characteristic refers to the distribution of Hα emission in two parallel bands, which move gradually apart during the main phase of the flare. Such flares tend to occur in relatively simple active regions, sometimes without spots; they are typically accompanied by very long-lived soft X-ray emission (Sheeley *et al.*, 1975), by type II radio bursts, by coronal transients, and by the production of interplanetary high-energy protons (Kahler *et al.*, 1978).

The most plausible explanation of the two-ribbon flare phenomenon yet advanced is that of Kopp and Pneuman (1976), who argue that reconnection of previously-opened magnetic field lines produces the continued heating necessary for the long-lived soft X-ray emission. Little direct evidence for this reconnection exists; P/OF observations would show the reconnection site as a weak X-ray enhancement and would provide emission-line diagnostic information about the plasma conditions occurring during the magnetic reconnection.

2.4 Microwave Bursts

Microwave emission as well as X-radiation gives information about the hot thermal plasma and nonthermal electrons in solar flares. Marsh and Hurford (1982)

have recently reviewed the new information coming from high-resolution microwave interferometers such as the VLA. The information provided by microwaves is quite different from that coming from X-radiation, both because of different emission mechanisms and because of different radiative-transfer characteristics. The chief differences are due to the effects of the magnetic field on the microwave emission. The hard X-ray emission mechanism is bremsstrahlung, produced when the 10 — 100 keV electrons are absorbed in high-density regions (thick target) or when they pass through low-density regions (thin target). The hard X-ray emission thus depends primarily upon the energy spectrum of the electrons and the local plasma density.

In the impulsive phase the microwave emission via the gyrosynchrotron process depends strongly upon the magnetic field strength as well as on the electron spectrum at higher energies (typically > 100 keV). Thus the microwaves give information concerning the quasi-relativistic electrons and so provide a "tracer" which follows the tail of the accelerated-particle population, while the hard X-rays reflect the lower-energy component that contains the bulk of the total particle energy. This is an important consideration, particularly in view of recent SMM and VLA results which show that the hard X-rays and microwaves are not spatially coincident (cf. Figure 1.2). P/OF will bridge the energy gap between SMM and *Hinotori* (typically $\leq$ 30 keV) and microwave ($\gtrsim$ 100 keV) observations.

In the gradual phase the microwave emission mechanisms are probably thermal: either free-free emission or gyroresonance radiation. In the latter case, the microwave spectrum will again depend sensitively on the magnetic field. In either case the microwave emission maps out magnetic trapping structures, but with different dependence upon the physical parameters. Simultaneous high-resolution imaging of both X-rays and microwaves therefore are complementary means for observing thermal, gradual-phase sources in solar flares.

Propagation effects also play an important role in the interpretation of microwave data: the sources are often optically thick. It is then difficult to determine the absolute number of accelerated electrons from the microwave spectrum alone. Since the X-radiation is optically thin, its quantitative interpretation is relatively straightforward. The X-radiation thus permits the electron population to be evaluated directly. X-ray and microwave imaging together can isolate the basic physical parameters — density and field strength — in the source regions.

2.5 Meter-wave Bursts

Numerous types of solar radio emission occur at meter wavelengths (e.g., Wild *et al.*, 1963; Kundu, 1965). These bursts (types I-V) are caused by nonthermal electrons accelerated in a variety of conditions, and the radio emission mechanism may be gyrosynchrotron, plasma-wave conversion, or free-free emission. In all cases, bremsstrahlung X-radiation should be generated and will define the source geometry in a way that has not been possible until now.

The X-ray observation of the solar corona outside of the flare proper is just beginning. The Skylab observations (Sturrock, 1980) and a long sequence of rocket flights have given us an excellent understanding of the morphology of the coronal soft X-ray sources. These sources consist of hot plasma trapped in closed magnetic loops both large and small. The prior observations have not defined the time variations of these structures in much detail, nor have they had the sensitivity to study the expanding corona on open field lines.

The hard X-ray observations of coronal nonthermal sources, known best up to the present from their meter-wave radio emissions, form one of the main objectives of the Pinhole/Occulter Facility. Accordingly section 4 of this report is devoted to this subject, including some of the recent results coming from the SMM and *Hinotori* spacecraft. Here we mention only the limb-occultation observations (Frost and Dennis, 1971; Hudson, 1978; Hudson *et al.*, 1982; Kane *et al.*, 1982) that unambiguously show the existence of coronal hard X-ray sources. In such observations the flare occurs at a longitude on the invisible hemisphere, well below (*e.g.* 25,000 km) the line of sight grazing the limb. Figure 2.5 shows an example of the stereoscopic observations in which the limb occultation clearly changes the detected X-ray spectrum. The occultation observations, and analyses that attempt to infer the coronal portion of the emission from whole-sun X-ray observations (*e.g.* Kundu *et al.*, 1982), provide indirect data at best.

2.6 Hot Thermal Sources

Recent observations with a high-resolution hard X-ray spectrometer (Lin *et al.*, 1981) showed that a relatively hot isothermal source occurred in a solar flare of 1980 June 27. Figure 2.6 shows the observed spectrum, which includes a hard nonthermal source as well as the softer thermal spectrum. Such hot sources should cool very rapidly by conduction, so their existence calls for a strong, continuous energy input or else a mechanism

(presently not understood) for confining the energy. The recent satellite observations (Hoyng *et al.*, 1981b; Tanaka *et al.*, 1982) suggest that such hot sources occur fairly commonly and may reach much higher temperatures than the 3×10^7 K observed by Lin *et al.* It is not known at present whether these sources are related to the flare X-ray loops whose cooling in the gradual phase produces the loop prominence systems seen in Hα. The imaging information from *Hinotori* indicates that these sources are compact, but little is known about their identification with other flare structures.

Figure 2.6—A hot (29.9×10^6 °K) isothermal component is evident in this hard X-ray spectrum from the solar flare of 27 June 1980 which was observed by a balloon borne instrument with ≈ 1 keV energy resolution. A power law component at high energies and a normal (14.5×10^6 °K) flare plasma were also present in this flare. The chi-square 90% confidence contour is also shown (Lin *et al.*, 1981).
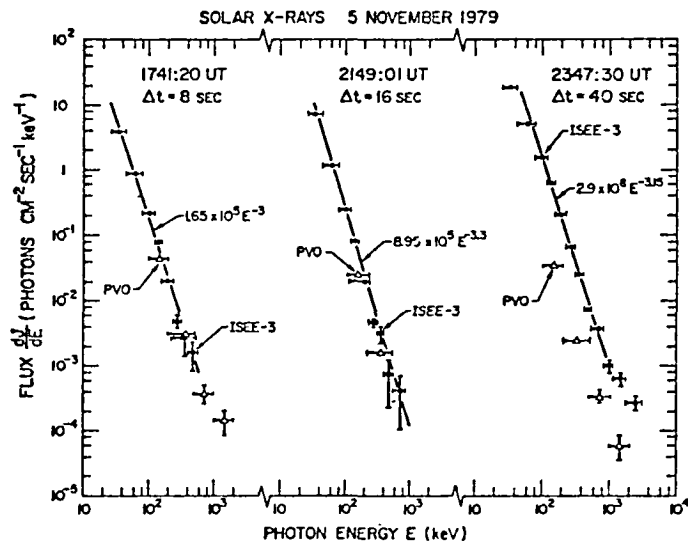

Figure 2.5—A comparison of the X-ray spectra measured by the ISEE-3 and PVO instruments at the time of three flares on 5 November 1979 (1741:20, 2149:01 and 2347:30 UT). Note the difference in the third of these "stereo" observations: the PVO points lie well below those of ISEE-3, showing that partial occultation occurred for this flare at the PVO location. In the third flare (2347:30 UT), part of the X-ray source at height ≥ 2500 km above the photosphere was occulted from the line of sight of PVO, which measured only ≈ 10% of the X-ray flux from the whole source measured with the ISEE-3 (Kane *et al.*, 1982).

Hard X-ray imaging observations of such soft sources can take advantage of the steep temperature dependence of the spectrum to separate the emission regions more effectively than soft X-ray observations, which have contributions from a broader range of temperatures.

2.7 Solar X-ray Observational Needs

To meet these scientific goals, the Pinhole/Occulter X-ray instrumentation must emphasize the following characteristics (roughly in order of priority):

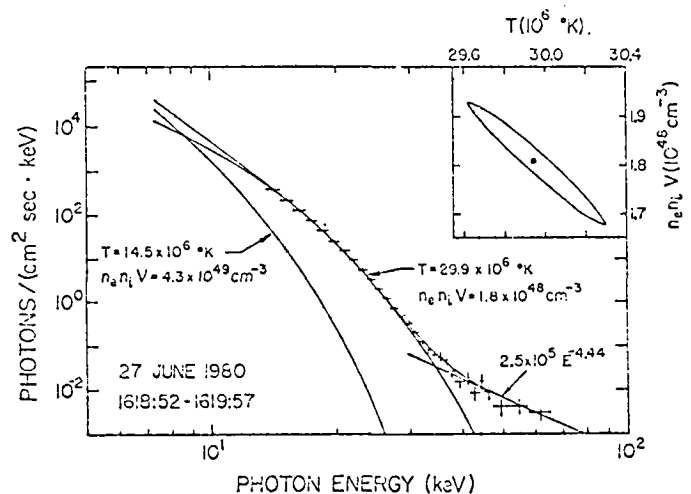1. *Response to hard X-rays.* The P/OF X-ray detectors must cover the hard X-ray band to high enough energies to characterize the hard X-ray spectrum adequately, both because many of the phenomena to be studied emit at these energies, and also because of the presence of bright and potentially confusing soft X-ray sources. In practice this means good response up to ~100 keV; response at still higher energies would also be valuable for direct comparisons to radio emissions.

2. *Spatial resolution.* P/OF must observe structures on the same size scales observable by SOT and the VLA, namely 0.1—1 arc sec. This corresponds to a few hundred km at the sun.

3. *Sensitivity.* Many interesting phenomena are likely to be quite faint, especially those related to the coronal phenomena discussed below. The sensitivity of the P/OF X-ray instrumentation should therefore be as good as possible, limited by counting statistics in a large-area counter. A flux sensitivity at 20 keV of 10^{-3} ph/cm² sec keV for a 10-sec integration on a point source is required.

4. *Dynamic range.* A solar flare may produce an X-ray flux 6-8 orders of magnitude above the background. The detectors must not saturate over this range.

5. *Time resolution.* The requirement for msec time resolution will be met by requirement (3), since the effective time resolution generally will be limited by counting statistics.

6. *Spectral range.* The instrumentation must effectively observe *soft* X-rays ($\geqslant$ 2 keV), since these delineate the magnetic structures of the corona in which the nonthermal phenomena and particle acceleration take place; the observations must extend up to $\sim$ 100 keV to observe the coronal nonthermal sources.

7. *Field of view.* P/OF will be much more efficient if the field of view of its X-ray imagers is large, since the location of solar phenomena cannot presently be well predicted. A field of view of 3 arc min for a single active region, and of the whole sun for coronal observations, is required.

8. *Observing interval.* Because interesting solar phenomena may be rare and unpredictable, the longest possible observing interval is desirable.

2.8 X-ray Instrument Concept

The development of imaging and detection systems to meet all of these sometimes-conflicting requirements has been the main challenge for the Science Working Group and its predecessors. An early tradeoff study by Hurford, together with considerable additional information, appears in the final report of the Hard X-ray Imaging Facility Definition Team. We will not dwell in detail on the analysis here, but simply describe the main technical conclusions and briefly discuss the rationale for each.

1. *Coded-aperture imaging should be used.* Focusing optics cannot presently give adequate high-energy response.

2. *A long "focal" length is needed.* To obtain high angular resolution, and to minimize the detector requirements, a long separation between occulter and detector is necessary. The model configuration uses a 50-m boom to create this separation.

3. *There should be two imaging systems.* The requirements for large field-of-view and excellent angular resolution tend to be mutually exclusive. The strawman configuration therefore includes both a Fourier-transform imager (Hurford and Hudson, 1982) for high resolution, and a coded-aperture imager for broad field-of-view.

4. *The detectors should be xenon-filled proportional counters.* Such counters are well developed, and much of the technology has been proven in numerous space applications (e.g. Rothschild *et al.,* 1981). They can be large in area and simultaneously obtain sufficient position sensitivity to permit the readout of the image information.

5. *A mechanical shutter assembly will be necessary to obtain a very large dynamic range.* This shutter will contain variable apertures with different effective filter thicknesses to reduce the low-energy solar flux.

The required characteristics of the X-ray imaging systems are listed in Table 2.1.

Table 2.1 X-ray Imaging Requirements

Coded-aperture Imager	
Angular resolution	8 arc sec
Field-of-view	whole sun (1°)
Energy range	2–30 keV
Energy resolution	10% (FWHM) @ 20 keV
Sensitivity in 10 sec	10^{-3} ph (cm^2 sec keV)$^{-1}$ @ 20 keV
Time resolution	1 msec
Fourier-transform Imager	
Angular resolution	0.2 arc sec
Field-of-view	3 arc min
Energy range	2–120 keV
Energy resolution	10% (FWHM) @ 20 keV
Number of subcollimators	100
Time resolution	1 msec

3. Coronagraphic Observations

3.1 Introduction

The concept of a Pinhole/Occulter Facility provides a unique opportunity to study the solar corona in a manner not available to stand-alone instrumentation. A large occulting system permits the use of large-aperture instruments; which offer both high spatial resolution and high photon collection rates from the intrinsically faint corona. These two major advantages will permit, for the first time, the study of small-scale phenomena in the corona and will provide sufficient sensitivity to carry out diagnostic analyses of intensities and line profiles for various coronal features, including the solar-wind acceleration region.

New plasma diagnostics using ultraviolet coronagraphic spectroscopy (Kohl and Withbroe, 1982; Withbroe et al., 1982) combined with coronagraphic observations at visible wavelengths can provide a powerful tool for describing the plasma physics of coronal structures out to beyond 8 R_o. Until recently coronal ultraviolet spectroscopy has been confined to the low corona within a few tenths of a solar radius from the solar surface. At higher levels coronagraphic observations have consisted, primarily, of very limited visible and IR forbidden line observations and broad-band measurements of the electron-scattered white light corona which determines only the electron density and the geometric structure of the multi-fluid coronal plasma. As a consequence, there has been very little information on coronal temperatures, nonthermal velocities, outflow velocities of coronal material to form the solar wind, coronal magnetic field strengths, chemical compositions and the spatial and temporal variations of these parameters. Figure 3.1 summarizes current measurements.

The available information has been insufficient to place significant empirical constraints upon the identities and functions of plasma heating processes, solar wind acceleration processes, mechanisms for transport of energy and momentum in the corona and processes for producing variations in chemical abundances. It also has not been possible to determine the role of different coronal regions in contributing to the outward flow of plasma into the solar wind or to determine the dominant physical processes controlling the evolution of coronal transients or the detailed effects of transients on the ambient medium.

This situation could be dramatically improved by the Pinhole/Occulter Facility which will permit extensive applications of new coronal diagnostic techniques for determining the basic plasma parameters of the corona including T_e, T_p, N_p, $V_{outflow}$, $V_{turbulent}$, plus the temperatures, densities and chemical abundances of coronal species other than electrons and protons. In some cases it may also be possible to determine coronal magnetic fields using Hanle effect measurements.
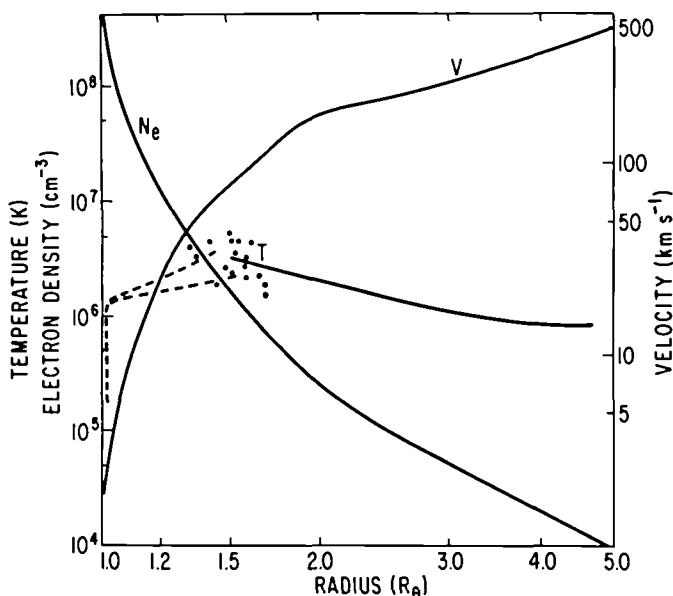

Figure 3.1—Sample physical parameters as a function of height in the corona. Quantities were obtained with low spatial resolution. Electron densities, N_e, were derived directly from white light observation of a coronal hole as were model-dependent outflow velocities, V. Electron temperatures at the coronal base (dashes) have been determined spectroscopically and a very limited number of ion (dots) and proton (solid line) kinetic temperatures have been obtained during eclipses and with a rocket coronagraph.

Limited applications of combined UV and visible coronagraphic diagnostics have already yielded low spatial resolution measurements of kinetic proton temperatures in coronal holes (Kohl et al., 1980) and in quiet coronal regions (Withbroe et al., 1982). These measurements which are based on observations of the line profile of resonantly scattered H I Lyman-α radiation and the white-light polarization and intensity have also provided an upper limit on the average outflow velocity of protons in 4 arc-min regions within 4 R_o of sun center. P/OF would permit these techniques to be applied with spatial resolution on the order of 1 arc sec or temporal resolutions on the order of 10 sec. Equally important, P/OF would. permit a very diverse set of plasma diagnostics to be applied using EUV observations in the 300 Å—1700 Å range with high spatial and temporal resolutions.

The unifying theme of the Pinhole/Occulter coronagraphic investigations is the *physics of coronal substructures*. In the past two decades, improvements

of the classical observational techniques expanded our knowledge to the point where simple models cannot adequately describe the sun's outer atmosphere: we must now consider inhomogeneous geometrical models such as loops, streamers, and coronal holes. These coronal features are distinguished by their different temperatures, densities, and magnetic field configurations. An unknown nonradiative energy flux interacts with the coronal plasma in each type of feature, and in essence controls its form. While with conventional UV and white-light coronagraphs we could distinguish some characteristics of coronal features at the largest scale, theory and models both demand a much finer spatial and temporal scale to discriminate among competing physical mechanisms which operate in the substructure of various coronal features.

Specifically the coronagraphic instruments on P/OF will concentrate upon the following scientific problems:

a. Understand the effects of processes that deposit energy and momentum within the substructure of the expanding corona and thereby generate the solar wind.

b. Understand the coronal dynamics of processes that deposit energy into the substructure of closed magnetic regions.

c. Understand the plasma processes occurring in adjacent closed and open magnetic-field structures.

d. Understand the interactive mechanisms of the plasma and magnetic fields as the corona reacts to slowly-varying conditions on the solar surface.

e. Understand the dynamic processes that are responsible for the expulsion of material from the solar surface in coronal transients and other ejecta.

The greatest potential for understanding the macroscopic physics of the various open and closed structures in the corona lies in the ability to apply plasma-diagnostic techniques at small spatial and temporal scales; this is the central observational thrust of the Pinhole/Occulter Facility. We describe in the remainder of this section the scientific questions addressed purely by the visible/UV coronagraph and the ultraviolet coronagraph/spectrometer. In Section 4, we address the joint X-ray/coronagraphic observations of the full set of instruments, which provide a very broad range of thermal and nonthermal diagnostics.

3.2 Scientific Objectives

The primary goal of the coronagraphic instrumentation of P/OF is to study the substructure of both open and closed magnetic field regions in order to understand the physical mechanisms which create, modify, and maintain the various types of coronal features. This broad objective can be logically broken down into five component parts, each dealing with either a common magnetic structure or a time scale over which the magnetic structure evolves.

3.2.1 Understand the effects of processes that deposit energy and momentum within the substructure of the expanding corona and thereby generate the solar wind.

In present spherically symmetric models of coronal expansion into the solar wind, energy is deposited in an *ad hoc* manner near the base of the corona. This deposition is usually in the form of thermal heating which is converted to kinetic energy of bulk flow as the material accelerates. But the corona is not spherically symmetric. We know coronal holes expand; these sources of high speed solar wind streams start as rather compact open field regions near the surface, and rapidly grow in area until they become major solar wind features. Particular attempts to model the high speed flow from coronal holes indicate that heating alone, even over an extended height range, cannot produce the needed acceleration to match the *in situ* observations obtained near earth. A direct deposition of momentum (e.g., by waves or turbulent inhomogeneities), perhaps combined with the rapid expanding geometry, seems to be indicated. These mechanisms can lead to the necessary acceleration very low in the corona (Zirker 1977, Jacques 1977, Hollweg 1978, Holzer 1979, Pneuman 1982).

However, the current models are almost unconstrained by observations; they use generalized properties and averaged parameters. Thus only broad statements can be made — such as estimating where energy input would be most effective in solar wind acceleration. It is not known what mechanisms actually heat the corona and drive the solar wind. We must first *find the location and extent of the deposition of energy and momentum in open field regions.*

It is not clear *what fraction of the corona is involved in the initial energy deposition.* We know that close to the sun, the most dynamic regions are centered in and over the chromospheric network. Here

spicules of relatively cool gas are expelled from the chromosphere and are heated as they merge into the corona. At the same time, transition-region observations (characteristic of plasmas on the order of 100,000 K) show general downflows over the network as well as display small impulsive events with both strong upward *and* downward motions (Brueckner 1980). The outflows could be the transition region counterpart of the chromospheric spicules. The material outflow in spicules and in transition-region plasma provides more than sufficient mass flux to replenish the corona from solar wind losses. In fact most of the mass returns to the sun in the form of downflows observed in transition-region lines. The dynamics of this mass flow appear to be on spatial scales of 1 arc sec or smaller. Clearly this mixing creates fluctuations in the magnetic field, and could be the site of "explosive" energy release. If this is truly the source of coronal heating and solar wind generation, then we might expect to see only a *small fraction* of the corona involved in the heating process in the low corona, and its effects would then propagate outward to fill a larger fraction volume at increasingly greater heights.

Once the location and extent of the nonradiative flux deposition can be observed, *does the effect of the magnetic field geometry and strength have a correlation to the effectiveness of the energy input*? Such a study may distinguish between magnetic wave-particle interactions and turbulent, dynamic, energy sources driven by mass motion. The tracing of the magnetic field and energy deposition would lead to a better understanding of the channeling and transport of energy converted from the nonradiative flux.

High-resolution temporal and spatial observations are needed to *ascertain whether or not the energy input to the corona is continuous or "transient" in nature*. The random nature of impulsive chromospheric spicule ejections and transition region expulsions of matter may create a highly localized, pulsed energy input. Signatures of such a process would be seen as intense heating and acceleration which then may dissipate as the ejecta spread to fill the outer corona. However, if the interaction is via magnetic waves, then maybe sub-surface convection motions would heat the corona more or less uniformly, or at least their energy input may be deposited along individual magnetic flux-tube substructures.

If turbulent fluctuations do exist, it may be possible to *identify the sources of interplanetary radio scintillation*. Plasma diagnostics performed on these features could link the coronal sources and production mechanism with observed fluctuations observed by the Helios spacecraft.

As part of the investigation to determine the physical energy deposition mechanism, we need to know *are there peculiar physical conditions which expedite the coupling of the nonradiative energy flux with the coronal plasma*? The plasma temperatures will certainly rise, but is there a preferential range of densities at the location of maximal energy input? Does the geometry of the magnetic field play an important role in converting the nonradiative energy flux into plasma signatures that are directly observable? Could reflection or wave-front interference be preferentially enhanced by the substructure of the magnetic field? Undoubtably, variations in the plasma characteristics exist where energy input is occurring, and these fluctuations will provide valuable clues about the physical processes responsible for the heating.

The properties of solar wind particles are strongly connected to the speed of the wind. Low-speed streams are characterized by low proton temperatures (a factor of 4 lower than electrons) and on occasion by a high helium abundance. On the other hand, high-speed streams have high proton temperatures (a factor of two higher than electron temperatures). Clearly the physical mechanism responsible for accelerating the solar wind in coronal holes interacts with the plasma in a different manner than the source of low speed wind. As heavy-ion *in situ* measurements are improved, we can expect even more information on the interaction mechanism. Such signatures should be directly observable in the corona. Preferential ionic heating, abundance changes, and ionic "freezing in" locations will present strict constraints on the possible heating mechanism. Thus the knowledge of the involvement of various ionic species in the heating and acceleration of the open magnetic field corona is of paramount importance.

From the above arguments, *monitoring the various ionic species should identify the coronal sources of low speed solar wind*. Because of the diverse 1 A.U. properties of low and high speed solar wind, low speed sources may be produced by an entirely different interaction mechanism. Thus it will be important to study other open magnetic field structures such as streamers, interstreamer regions, and the open areas of active regions — especially their contrasting characteristics and properties compared to corresponding ones for coronal holes.

3.2.2. Understand the coronal dynamics of processes that deposit energy into the substructure of closed magnetic regions.

Most of the strong X-ray, EUV and visible forbidden line emission from the lower corona is produced in closed magnetic regions, and more particularly, from individual flux tubes. Such tubes or loops of small scale and high intensity are found in ephemeral regions, larger loops emanating from active regions, and loops of larger scale in the quiet corona interconnecting active regions or bridging between organized regions of opposite magnetic polarity.

Considerable recent theoretical effort has been applied to the physics of loops. Quasi-static loop models in energy balance seem capable of explaining many observed gross properties of hot active region loops. Unfortunately these models are not very sensitive to the heating mechanism assumed and current observations do not seem adequate to set firm constraints on possible heating mechanisms. The general scientific goals concerning loop structures will necessarily stress the larger scale systems, although with the proper mechanical design of P/OF and associated coronagraphic instrumentation, it should be possible to observe most features almost to the limb and even onto the disk for the shorter-wavelength instruments.

As with the discussion on open field lines in the corona, we need to *locate and define the extent of heating and dissipation in loop structures*. In most cases, the tops of loops appear hotter, possibly because their lower density is incapable of adequately cooling the plasma through radiation, or because the energy input mechanism preferentially selects this portion of the geometrical structure for its maximal release. There are two other possibilities, however, to explain the energy balance problem in the loops. The radiative, conductive, and bulk-flow energy transport may be so efficient that the specific heating mechanism is unimportant in determining the observational properties of the loop as a whole. Finally, the apparent observational parameters may merely reflect the existence of an ensemble of a number of unresolved substructures, each with its own particular well-defined properties and physical mechanisms.

Most of the mechanisms considered for heating coronal plasma loops fall into several classes:

a) **Anomalous dissipation of currents.** Coronal loop systems must be very nearly force free, but are not necessarily potential. Even small departures from potential configurations can produce currents capable of heating the corona.

b) **Alfvenic disturbances.** Generated by convection motions below the photosphere, the continual stressing and motion of the magnetic field induces twists, surface waves and body waves that propagate *along* flux tubes to heat individual, and at times apparently isolated loops.

c) **Fast Mode MHD waves.** With their energy supply similar to that of the Alfvenic disturbances, fast mode waves need not propagate along the magnetic field structure of the loop and this may be responsible for a more widespread generalized heating of the corona than its more confined counterpart.

d) **Small scale magnetic reconnection.** The "salt and pepper" field structure at photospheric levels, especially in network regions, may reconnect with the larger scale loops, sending energetic particles and waves along the resultant large scale loops as they dissipate their energy into the coronal plasma. There is considerable evidence that this mechanism occurs, although large scale reconnection is presumably not important for *static* loops.

In most of the above mechanisms, the problem lies in finding an adequate dissipation mechanism. A number of such mechanisms have been studied (see review by Hollweg 1981) but their predicted signatures are difficult to observe as the dissipation processes may occur on very small spatial (and temporal) scales.

Early studies of active region loop structure show both variable temperature loops and nearly isothermal loops coexisting in the same general coronal structure. *Why is there an apparent thermal isolation and differentiation of adjacent loops?* Different heating mechanisms may dominate individual adjacent substructures in loop systems because their connection to the photosphere and chromosphere represents entirely different physical conditions. Thus the sub-arc sec surface structures may have a profound influence on coronal loops at a correspondingly small scale. A recent analysis by Dere (1982) of Skylab data shows a general trend for the most intensely emitting loops to vary in temperature throughout an active region. However, the observations are insufficient to resolve individual substructures (filling factors are much less than unity). We need to know *how the physical properties of individ-*

ual loops depend upon their photospheric origin. Is there a real distinction, either through the gross plasma characteristics of their photospheric connection (e.g., active regions or large-scale unipolar regions) or the inferred complexity of the magnetic structures, among loops of different spatial scales? If the physical characteristics of active region loops can apparently be so different, then does this same phenomenon exist for the largest-scale features such as the closed magnetic-field structure of streamers or interconnecting active region loops?

A specific example of this phenomenon is the dark cavity observed to overlie prominences but surrounded by the bright structure of a streamer. Because only the density contrast is presently known, we assume the supporting forces are produced by an increased magnetic field strength and/or an increased coronal temperature in the cavity. Also unknown is why the demarcation between the cavity and the classical helmet structure is so sharp. Does the scale of the loops effect the energy generation mechanism such that the mass is allowed to drain from these particular loops? Once the plasma properties of these cavities are known, we can then attack questions as to why these loops are so physically different from their surroundings. While all energy input mechanisms may exist simultaneously, we need to ascertain what physical conditions are required for a unique mechanism to be the dominant source of heating.

3.2.3 Understand the plasma processes occurring in adjacent closed and open magnetic-field substructures.

The previous discussions have treated open and closed magnetic-field regions as separate entities. But are the energy-deposition mechanisms really fundamentally different? The apparent differences between these two types of features may simply be controlled by the geometry of the magnetic field. In one case the coronal plasma is confined and restricted; the other permits a substantial energy release mechanism through organized bulk outward flows. A test of this hypothesis is best conducted on features whose energy input, both in form and magnitude, can be as similar as possible. Thus the appropriate coronal area would be located in adjacent closed and open magnetic-field regions.

The most easily observed circumstance is the change from closed to open field lines in coronal streamers. The photospheric origin of this interface presumably lies far from the neutral line in essentially nondescript and "homogeneous" regions of the sun.

Thus the nonradiative energy flux from below should be the same and any differences in the corona should be due to magnetic geometry.

On a smaller spatial scale, there may be peculiar plasma effects at the interface between open and closed field lines. Current sheets may be present; shear in bulk flow may exist. The types of phenomena that might be present are probably on a small scale.

3.2.4 Understand the interactive mechanisms of the plasma and magnetic fields as the corona reacts to slowly varying conditions on the solar surface.

The previous discussion focused upon the steady-state nature of the corona, including the flow in open field lines and inhomogeneities that might be propagating in the substructure of coronal features. Because the corona's existence is dictated by the nonradiative energy flux and the magnetic field protruding through the photosphere, it then must react as conditions slowly evolve at the solar surface. The random motion of granulation will move the magnetic field foot points, creating currents and modifying coronal structures.

As the coronal structures change, is there a continual evolution of plasma properties and geometries or do dynamically unstable processes dominate? For example, coronal loops within active regions are often quite stable in spite of obvious photospheric and chromosphere changes. Nevertheless the loops do evolve and sometimes develop rapidly. Foot point motion may imperceptibly modify a loop's geometry, with the plasma properties slowly adjusting to compensate for the new conditions. This will alter radiation, conduction, and enthalpy losses and may change the amount of heating, and hence produce further modifications of conditions within the loop. Such slow evolution may occur most of the time in loop structures (moving from one quasi-equilibrium state to another), but its importance to the form and nature of the surrounding corona is unknown. The same phenomena may occur in open field structures, but presumably to a lesser extent.

However, if the conditions are such that thermal and/or MHD instabilities occur, then radical changes on a short time scale would be expected. Once a dynamically unstable process has been initiated, we would like to know *what physical processes occur as the loop dynamically evolves. Can the final state of the corona be predicted from the initial conditions?* If, for example, the density in a coronal loop were

increased to a point where it would radiate more energy than could be supplied, the temperature would drop, resulting in further increased radiative losses and possibly producing, in the final state, the observed cool coronal loops in active regions. During the times when the physical conditions dramatically change, *does the coronal heating mechanism also change?* This question relates back to the study of heating mechanisms for different conditions of stable magnetic field substructures. If there is more than one dominant coronal heating mechanism, then we may learn more about the relative importance of the different processes by studying the changes in individual structures (rather than a statistical study of homologous features).

As part of the dynamics of surface magnetic field evolution on coronal forms, we wish to know *how mass is redistributed as the magnetic field changes.* Stimuli could either come from changes in the mass injection mechanism at the base of the foot points or in redistribution due to changes in the magnetic field geometry or heating source. Generalized flow in both loops and open magnetic structures has been observed, *but the mechanisms that drive the flow are not known.* Flows within uniform and expanding magnetic field geometries have been studied theoretically, but thus far there have been very few observations capable of subjecting the theoretical work to observational test. Since even small pressure differences between the two foot points of a loop will drive siphon flow, we expect flows within loops to be common. If the flows are not initiated at the base of the loops, then *do thermal and/or MHD instabilities in the upper regions of the loop (created by photospheric magnetic field motions) trigger such flows?*

3.2.5 Understand the dynamic processes that are responsible for the expulsion of material from the sun in coronal transients and in other ejecta.

Observations from Skylab and more recently from SMM, the P-78 satellite, and from the ground-based Mark III K-coronameter show that coronal transients observed in white light (and in other emissions) are a common phenomenon and may account for as much as 10% of the total solar mass loss. These observations (Figure 3.2) show that the disturbances are often looplike in appearance, and their trajectories imply a continued propelling force. Other transient events can be described as initially voids slowly moving outward through the corona, material being injected into pre-existing structures such as streamers and rays, and
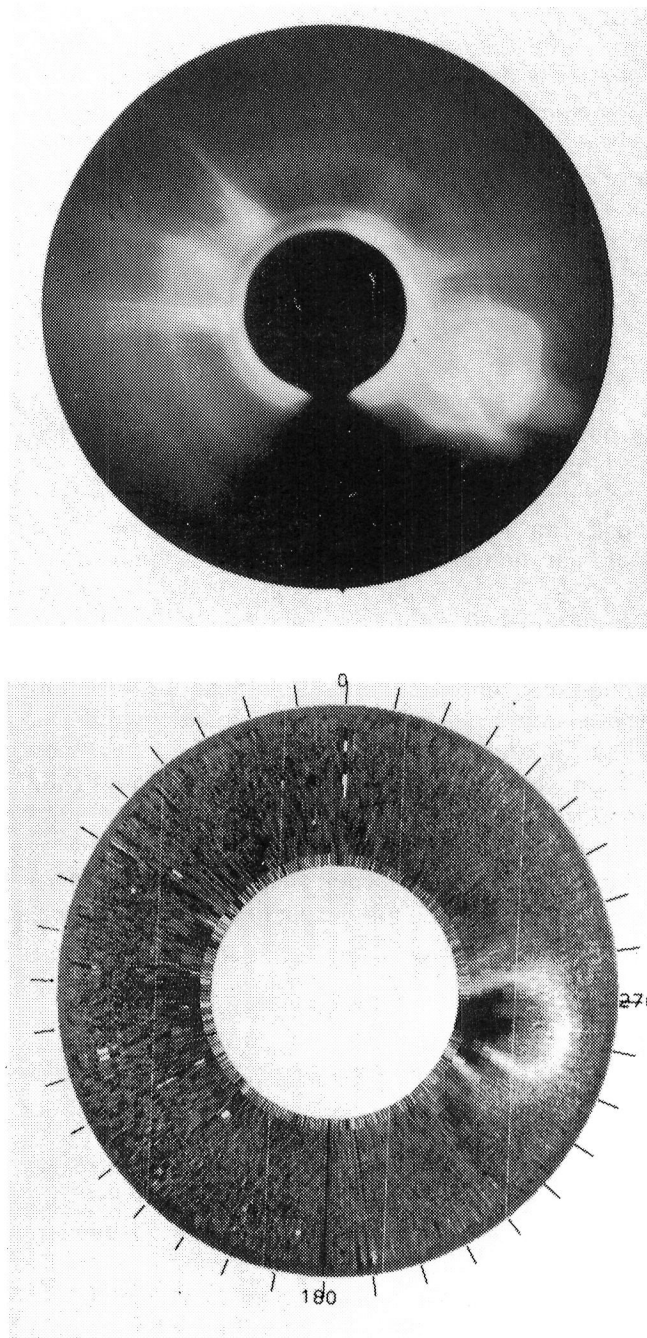
Figure 3.2—White light coronal transient observations obtained from a ground based K-coronameter (top) and a space borne coronagraph (bottom). P/OF observations of these events will permit complete plasma diagnostics, including for the first time temperatures, at resolutions of from 10 to 20 times those depicted in the figure.

finally a class of events where the coronal magnetic field is apparently rearranged, with mass being ejected outward into the solar wind as a consequence. Transients are most closely associated with the eruption of filaments; flares seem to be a secondary source, and are associated only when material is ejected (in the form of

an eruptive filament or flare spray) from the flare site. Presently, observations have been limited to white light, H alpha, the F XIV green line (in the low corona), and radio emissions (Type II, III, and IV's). Hence we know little about the other plasma properties except the temporal history of the mass, geometry, and apparent gross velocity characteristics. There are no observations on temperature (other than sometimes in small interior regions where eruptive prominence material still exists), no direct determination of the velocity of outflowing material on any spatial scale and no information on mass flow within individual magnetic substructures.

At the present time, the mechanism of transient expulsion is in dispute; many theoretical efforts to understand this complex phenomenon in terms of different dynamical models have been initiated during the past few years. Although progress has been made, many important questions of the physics of coronal transients remain outstanding. One fundamental question concerns the *circumstance under which a transient eruption is initiated in the low corona*. It is firmly believed that the magnetic field is linked to the initiation of such events and most certainly in its dynamic passage outward through the corona. One of the problems facing the interpretation of the observations today is the wide variation of the nature of the events: velocities of the leading edge of transients covering more than an order of magnitude (50 to over 1300 kms^{-1}); geometries of the magnetic field and mass distribution assuming various forms (from a loop like appearance to injection of excess mass into pre-existing coronal streamers and rays); and the possible inclusion of prominence material in the interior portions of the transient (which can either undergo heating and ionization as it rises outward or be essentially isolated from processes that would change its form). The more spectacular and energetic transients have close correlations to large flares with their associated filament eruptions. Impulsive phenomena (such as a pressure pulse resulting from emerging magnetic flux, from magnetic reconnection, or from a plasma instability) may best describe the origin of these events. At the other end of the transient spectrum, slow moving, initially depleted volumes propagating outward from the sun may result from quasi-static evolution of the surface magnetic fields that eventually become unstable and rise due to forces such as magnetic buoyancy.

Clearly, the role played by the magnetic forces in the corona which activate such a wide spectrum of coronal transients needs to be investigated. Are there in fact different circumstances which produce coronal transients, e.g. initiation by an "explosive" realignment of the

magnetic field as in a flare or alternatively through slow evolution of the general magnetic structure of the sun? Is there a change in the characteristics or magnitude of the coronal heating mechanism prior to a mass ejection that may serve as the catalyst for magnetic involvement? Does magnetic-field reconnection affect and/or produce coronal transient expulsion? How does the liberated energy and new magnetic field configuration interact with the surrounding plasma and expel it from the sun? Finally, does the outward convection of magnetic-field energy in a transient dominate the energetics of the solar flare that produced it (e.g. Webb *et al.*, 1980)?

These questions touch on just a few of the unknown dynamic processes which initiate and propel material from the sun in the form of coronal transients. In section 4 we describe scientific objectives relating to the investigation of particle acceleration in the corona These require the simultaneous use of both the hα X-ray and coronagraphic instrumentation of the Pinh Occulter Facility.

3.3 Coronagraphic Observational Requirements

The scientific objectives require two instruments. The visible/UV coronagraph will measure the intensity and polarization of broad band visible light and will obtain coronal images at selected visible and UV wavelengths. The ultraviolet coronagraph-spectrometer will be used for spectroscopic work within the 300 Å— 1700 Å range (ultimately this range should be extended to shorter wavelengths). The observational considerations for the two types of instrumentation are discussed separately, where necessary, in the following (roughly in order of priority):

3.3.1 Orbital Altitude

For acceptable atmospheric attenuation of solar radiation at ultraviolet wavelengths, the coronagraph should operate at an altitude of ⩾400 km.

3.3.2 Stray Light Rejection

Ultraviolet Coronagraph-Spectrometer

External occultation is essential in ultraviolet coronagraphic instruments, otherwise the inherent surface scatter in mirrors would completely mask all but the innermost coronal regions. An internal occulter must also be used to intercept diffracted light from the external occulter. Requirements for on-band and off-band

wavelengths must be met that are somewhat different for the various spectral lines of interest. For a signal (from coronal radiation) to noise (from stray light) ratio ≥ 10, the on-band stray light rejection required for the resonantly scattered H I Lyman-α line is 10^{-7} to 10^{-8} for observations out to $\rho \approx 4\,R_0$ and about an order of magnitude better for measurements beyond $\rho \approx 6\,R_0$. Requirements for observations of other resonantly scattered lines is about an order of magnitude less stringent and observations of the broad electron-scattered component of H I Lyman-α requires about an order of magnitude more rejection. The required rejection of off-band radiation at visible and near UV wavelengths is critical because the solar photon fluxes are extremely large. Normal incidence telescope-spectrometer systems without occulting systems that have been flown on spacecraft have had stray light rejections of the order of 10^{-3} (e.g. Harvard Skylab, OSO-4 and OSO-6 EUV instruments). For H I Lyman-α, this was inadequate for observations at all heights above the limb. For coronal lines like Mg X $\lambda 610\,\text{Å}$, observations of some coronal structures up to $\rho \approx 1.4\,R_0$ may be possible without external occultation.

Visible/UV Coronagraph

Both external and internal occultation is essential in the visible/UV coronagraph to reduce the instrumentally produced stray light. Requirements are most strict in the visible where signal levels are approximately 1×10^{-8} to 1×10^{-10} times that of the radiation from the solar disk. The primary source of instrumentally produced light is from the diffraction pattern from the external occulter and body scatter from the surface of the telescope primary. •

3.3.3 Sensitivity

The sensitivity of any coronagraph is set by the unvignetted collecting area of the occulted telescope, the efficiencies of the optical components and the efficiency and position-sampling capability of the detection system. Technical considerations aimed at improving the optical efficiencies and the detectors will be discussed later in this section.

An externally occulted coronagraph vignettes the incident coronal light with the degree of vignetting dependent upon the radial height in the corona. The action of the vignetting may be visualized in the following way: rays emanating from the outermost (unvignetted) coronal regions have an unimpeded path to the telescope primary, and effectively ignore the presence of the

external occulter. However, rays from coronal regions closer to the solar limb only illuminate an unshielded portion of the coronagraph-telescope. The innermost coronal rays that can reach the telescope illuminate a vanishingly thin strip near the telescope-mirror edge. The unvignetted area available for an observation at a particular heliocentric radius is proportional to the distance between the external occulter and the telescope minus the amount of over-occulting — the ultimate area being available during a natural solar eclipse, but only for a very brief period of time.

P/OF will provide a long boom which can be used to separate the external occulter from the telescope. The large separation provides the possibility of using a large aperture telescope which can be shielded from solar disk radiation by the distant external occulter. The occulted telescope provides a large unvignetted area for observations of coronal regions with small angular separations (corresponding to $\rho = 1.2\,R_0 - 10\,R_0$) from the bright disk.

Ultraviolet Coronagraph-Spectrometer

The unvignetted area is the major technical problem that limits the practicable spatial, spectral and temporal resolutions of the photon-starved ultraviolet spectroscopic observations. Figure 3.3 depicts expected intensities as a function of radial height in the corona for resonantly scattered and collisionally excited components of several spectral lines. The intensities are based on the maximum equatorial model given by Allen (1963). A conventional size instrument such as the one defined for Spacelab (Kohl et al., 1981) would yield a count rate of $\approx 10\,\text{Hz}$ per resolution element at the center of the spectral line profile for an integrated line intensity of 5×10^7 photons/$(\text{cm}^2\,\text{s str})$ (using a spatial resolution of $0.15' \times 4'$ and spectral resolution $0.1\,\text{Å}$). The same observation with the P/OF occulter and a 44 cm telescope would yield a factor of 20 higher data rate which could be used to improve the temporal resolution. Alternatively, the spatial resolution could be improved to 2 arc sec $\times$ 10 arc sec while maintaining the original data rate. This improvement is typical for measurements where a high spectral resolution requirement (i.e. the spectrometer entrance slit width) sets the spatial resolution in one dimension. For low spectral resolution measurements (2 Å), such as measurements of the broad electron scattered profile of H I Lyman-α, integrated line intensity measurements and Hanle effect measurements (i.e. linear polarization of line intensity), a factor of 88 improvement in data rates will be obtained for observations with better than 36 arc sec spatial reso-

lution. Alternatively, the same factor can be used to improve the spatial resolution. These improvements make it possible, for the first time, to investigate the magnetic substructure of the acceleration region, and will provide a broad set of plasma diagnostics as well as provide the time resolution needed to measure the plasma parameters of active regions, flares and coronal transients.
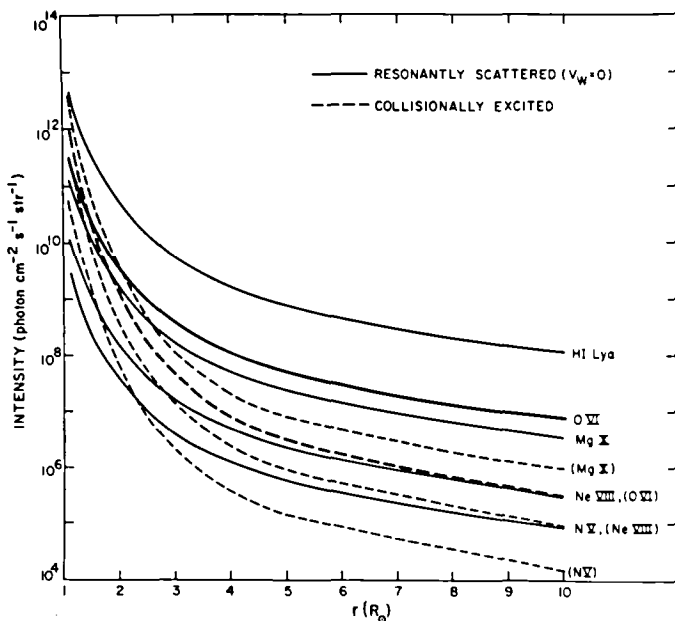

Figure 3.3—Static corona intensities of collisionally excited (*dashed lines, ion name in parentheses*) and resonantly scattered (*solid lines, ion name without parentheses*) components of prominent coronal constituents.

Visible/UV Coronagraph

Using typical values of broad-band measurements in the corona, the increase in collecting area of the telescope (50 cm diameter vs 3 cm for coronagraphs flown on the ATM Skylab and SMM missions) permits observations from the P/OF at a resolution of 1 × 1 arc sec at exposure times (in the visible) of 1 to 60 seconds, depending upon the spectral bandwidth used to isolate coronal emission lines. Conventional instrumentation could only obtain information at spatial resolutions of 8 to 12 arc sec with exposure times of 10 seconds to tens of minutes. The improvements which can be obtained with the P/OF instrumentation will permit the investigation of the corona on a spatial and temporal scale not attainable by stand-alone coronagraphs.

3.3.4 Spatial Resolution

To meet the scientific goals discussed in section 3.2, the P/OF coronagraphs must resolve the magnetic

structure of closed magnetic field regions such as coronal streamers and also resolve the structure of open magnetic field regions such as coronal holes. Spatial resolution on the order of an arc sec combined with differencing techniques to remove background and with high time resolution is needed to discover the coronal substructure's contributions to solar wind acceleration. High spatial resolution (1—10 arc sec) is required to determine the plasma parameters of regions where particle acceleration originates, and to study coronal areas above these regions that are disturbed near the time of such events and give rise to coronal vacancies and transients. Observations of particle acceleration are discussed in section 4.

3.3.5 Temporal Resolution

Ultraviolet Coronagraph-Spectrometer

This requirement is dependent on the sensitivity since the effective time resolution generally will be limited by counting statistics. Ideally, this requirement should permit an appropriate field-of-view to be scanned in less time than it takes for the average conditions within a spatial resolution element to change. For many coronal structures, a time resolution of 10 minutes or more will be acceptable. For observations of coronal transients which have apparent velocities of 300—700 km s^{-1}, a field of view extending up to 3 R$_o$—4 R$_o$ should be sampled in a few seconds in order to preserve a spatial resolution of a few arc sec within this range. P/OF should provide measurements of the H I Lyman-α line profile and of other spectral lines. For shorter duration events, it may be desirable to hold the coronal image at one position and accumulate data at resolution elements along a strip which corresponds to the spectrometer slit. In certain cases, the temporal resolution is related to the pointing stability because the instrument spends time observing outside the spatial element of interest. This effect is minimal for observations which require a full raster of a spatial region that is larger than the pointing instability.

Visible/UV Coronagraph

The normal cadence of observations will be approximately one 1000 × 1000 CCD image of the corona every 5 seconds. Using 12 bits per pixel, a data rate of 2.4 MBps would be needed to record the information. Thus intelligent onboard data processing must be applied to the data before shipment to the ground. Thus the operational constraint of data recording or transmission will be the limiting factor for the highest temporal image cadences.

3.3.6 Wavelength Range and Spectral Resolution

Ultraviolet Coronagraph-Spectrometer

An empirical description of solar wind generation and of the characteristic behavior and structure of the corona requires a determination of the parameters (temperatures, densities, turbulent and flow velocities) of the major constituents of the multi-fluid coronal plasma and a determination of the magnetic fields. A key to understanding the basic physics of the corona is to observe the effects of wave propagation and of unknown energy and momentum deposition processes on the spectra of coronal particles of different mass in order to discover the identities of the dominant processes involved. The appropriate plasma diagnostics require measurements of the intensities and profiles of spectral lines over a broad wavelength range. Technical considerations (discussed later in this section) suggest that the 300 Å—1700 Å range would be appropriate as a first step — ultimately the range should be extended to shorter wavelengths. Spectral line profiles for the more massive particles of interest are expected to be about 0.2 Å FWHM requiring a resolution in the EUV of $\approx$10,000.

Visible/UV Coronagraph

Because the visible/UV coronagraph will be a reflecting optical system, the full range of about 1700 to 11000 Å is accessible for detection. This type of design permits the use of dielectric filter techniques to isolate individual coronal spectral lines as well as broadband measurements of the electron scattered continuum. Spectral resolution of individual lines depends upon tunable filter systems and the sensitivity of the CCD detection system.

3.3.7 Field of View

Ultraviolet Coronagraph-Spectrometer

The field-of-view of the coronagraph-spectrometer should be large enough to track coronal phenomena in radial directions out to at least 8 R_o and in the perpendicular direction it should accommodate simultaneous observations across the full extent of typical coronal structures ($\leq$10 arc–min). The P/OF should be capable of rolling the ultraviolet coronagraph-spectrometer and occulter together about sun-center in order to permit coronagraphic observations along any radial direction.

Visible/UV Coronagraph

The simultaneous field of view for the visible/UV coronagraph is limited by the CCD detector array size at a 1 arc sec resolution. Present technology can provide an image size of .5 × .5 R_o at this spatial resolution; future 1000 × 1000 CCDs up the field of view to 1 × 1 R_o. Thus for a complete picture of the corona, a series of images (formed by an internal articulating mirror) is required to produce a mosaic composite.

3.3.8 Observation Interval

Because solar phenomena are difficult to predict and because some faint sources will require long data accumulation times, the longest possible observing intervals are desirable. The ultimate capability of coronagraphic observations would be achieved with a P/OF facility in long-term orbit to study the temporal and spatial variations in physical conditions throughout the lifetimes of a large set of coronal structures.

3.3.9 Contamination Effects

Coronagraphic instrumentation is designed to observe the weak intensity of coronal radiation while simultaneously rejecting solar disk radiation. The angular separation between the radiation emanating from the observed coronal regions and that originating from the intense solar disk will be between 1.6 arc minutes and 2 degrees depending on a region's angular position. Contaminants located in the bright sunlight along the coronagraphic line-of-sight can scatter light through the instruments to the detectors. Both particulate scattering and Rayleigh scattering are of interest. In general, the equivalent of a class 10,000 clean room condition is acceptable. In addition, atomic and molecular contaminants can attenuate incoming ultraviolet radiation. Return fluxes of contaminants could result in deposition of substances onto optical surfaces which may act as radiation scatterers and/or absorbers. Open photoelectric detectors used for wavelengths shortward of 1050 Å require an ambient pressure in the immediate vicinity of the detector of less than 10^{-5} torr for ideal operation.

3.3.10 Technical Enhancements

Although coronagraphs could be built for the P/OF instrument plane using existing technology, the following are several technical considerations that could enhance the observations:

1. EUV Array Detectors

The ultraviolet coronagraph-spectrometer will benefit from two dimensional array detectors currently under development. An appropriate detection system should have high counting efficiency at EUV

wavelengths, cover a 10 × 40 mm area with ≤10 μm resolution elements, be insensitive to wavelengths >1800 Å and meet requirements for low dark counts, dynamic range and stability.

2. Serrated Edge Occulters

The degree of stray light rejection of a coronagraph is directly proportional to the amount of solar disk radiation that is diffracted by the external occulter onto the telescope mirror. Serrated occulters would have a saw toothed edge designed to direct diffracted light away from the telescope mirror surface. This directly reduces the primary stray light level which results from the non-specular reflection, by the telescope, of occulter-diffracted light into the spectrometer entrance slit or the CCD of the visible/UV instrument. (The internal occulter intercepts diffracted light that would otherwise be specularly reflected into the spectrometer or detection system.)

3. Optics

Developmental multilayer dielectric coatings could be used to improve substantially the normal incidence reflectance of optical surfaces, thereby improving the radiometric efficiency in the 300 Å—1700 Å range and ultimately extending the range for normal incidence optics to shorter wavelengths. The ultraviolet coronagraph-spectrometer would benefit from the development of large toroidal or ellipsoidal diffraction gratings which would sharply reduce the aberrations of single reflection systems. The use of dielectric filters for the visible/UV coronagraph has been covered in section 3.3.6. A critical requirement is the visible light rejection of UV-transmitting filters. Both coronagraphs may also benefit from advances in mirror polishing techniques which could be used to reduce the non-specular reflection by the telescope mirror of diffracted light from the external occulter. It has been shown that the main contributor to mirror scattering is not the coatings (unless they are non-uniform) but the subsurface polish.

The observing program necessary to accomplish the scientific objectives would include simultaneous and co-spatial observations with a visible/UV coronagraph and an ultraviolet coronagraph-spectrometer. For observations of active regions, coordinated observations with P/OF's hard X-ray instruments are needed. The visible/UV instrument would observe primarily the intensity and polarization of visible light and the ultraviolet coronagraph-spectrometer would measure the line profile, intensity and, in some cases, the linear polarization of coronal radiation in the 300 Å—1700 Å range.

Together, the two instruments would determine the basic plasma parameters and geometry of coronal structures associated with open and closed magnetic field regions between 1.2 R_o and 10 R_o from sun center. The visible/UV instrument would also obtain coronal images at selected visible and UV wavelengths and continuously monitor the visible corona throughout a wide field-of-view extending 120° about the disk. The ultraviolet coronagraph-spectrometer would use internal telescope motions to raster segments of the corona. For observations of active regions and coronal transients, the coronagraph-spectrometer would benefit from external monitoring information that would permit it to track active region phenomena. This information might come from P/OF's hard X-ray or visible light observations.

The length of the observing interval should be as long as possible to observe a suitable sample of coronal structures and events. A one-week Spacelab flight would provide a significant amount of data. To study the longer term evolution of the corona, the P/OF coronagraphs will eventually require a free-flying observing platform such as the Advanced Solar Observatory.

Table 3.1
Coronagraphic Observational Requirements

Ultraviolet Coronagraph-Spectrometer

Wavelength range	500 Å—1700 Å (initially) 50 Å—1700 Å (ultimately)
Spectral resolution	10,000 (in EUV)
Angular resolution	1 arc sec
Field-of-view	1.2 R_o to 10 R_o in radial direction and 30 arc min tangent to limb (using internal rastering) 360° about sun center (by rolling P/OF)
Time resolution	≈10 sec
Telescope aperture	44 cm × 44 cm

Visible/UV Coronagraph

Wavelength range	1100 Å—11,000 Å
Spectral resolution	Dielectric Bandpass Filters
Angular resolution	1 arc sec
Field-of-view	1.0 by 1.0 R_o simultaneously 1.2 to 10 R_o in radial direction and 3 R_o tangent to limb (using internal rastering) 360° about sun center (by rolling P/OF)
Time resolution	≈1 sec
Telescope aperture	50 cm diameter primary

4. Coronal Particle Acceleration

4.1 Introduction

The combination of coronagraphic and X-ray instrumentation gives us the means for simultaneously observing coronal nonthermal phenomena (particle acceleration) and the detailed physical properties of the unstable plasmas.

The solar corona may be the ideal place to study the acceleration of high-energy particles and their energy-dissipation processes in a magnetized plasma. These phenomena appear to be ubiquitous in active plasmas elsewhere in the universe. Radio observations at meter wavelengths have shown that a wide variety of particle-acceleration processes occur in the corona (Wild et al., 1963). The metric radio observations themselves provide little quantitative data on the particle-acceleration processes, since the radiation processes are generally complicated and not well understood. In addition, scattering and absorption of the radio waves in the corona limit the determination of the location and sizes of the metric radio sources to a few arc minutes. With the unique capabilities of the P/OF for high sensitivity and high spatial resolution in X-rays, white light, and EUV, it will be possible for the first time to provide physically significant constraints on these acceleration processes. The P/OF instrument complement will allow us to observe the nonthermal phenomena with an ideal array of diagnostic tools, both for the nonthermal particles and for the essentially thermal background plasma.

The high-sensitivity P/OF hard X-ray observations will be able to provide precise locations and sizes (to a few arc seconds) and also numbers and energy spectra for the fast electrons accelerated in the corona. The X-ray instrumentation will be sensitive enough to detect and follow even weak type III bursts at coronal densities of 10^6 cm^{-3}, equivalent to heights of $2R_0$ above the solar surface. The visible/UV coronagraphic observations will show the overall coronal thermal electron density structure in which these fast electrons are accelerated and through which they propagate, to arc-sec resolution. In particular, changes in the ambient-electron density structure will be detectable on time scales (< 1 sec) relevant to these acceleration processes. The ultraviolet coronagraph-spectrometer will provide detailed diagnostics (Kohl et al., 1980) of the acceleration region at a few arc sec resolution: measurements of T_e, T_p, n_p, the bulk flow velocity and nonthermal ion velocities. Well-ordered flows might be expected for magnetic merging, while nonthermal ion velocities may indicate the pres-

ence of turbulence or waves. A very promising possibility is the measurement of the coronal magnetic field strength and direction via the Hanle effect (Sahal-Brechot, 1974), which produces a depolarization of the resonance-scattered radiation observed by the EUV coronagraph. In turn, by following the fast electron sources in hard X-rays as they travel outward, it will be possible to trace the magnetic topology of the coronal structures. Furthermore, hot spots in the corona where energy dissipation is taking place can be seen in thermal soft X-rays. Such hot spots might occur where the coronal structure is evolving via magnetic merging or current dissipation. Also with the quantitative measures of the energetic electrons provided by the hard X-ray imaging and the diagnostics of the ambient medium from the coronagraphs, together with the interplanetary observations of particles and low frequency radio emission, it will be possible to identify the metric radio emission processes and to study quantitatively the beam-plasma interactions that are likely to occur.

4.2 Type III and V and U Bursts

Type III bursts are the most common type of impulsive nonthermal phenomena occurring on the sun. They exhibit rapid frequency drift from high to low frequencies (Wild et al., 1963). Simultaneous in situ particle and low-frequency radio observations from spacecraft at 1 A.U. have confirmed that Type III bursts are caused by electrons of about 5—100 keV energy that escape from the sun after an impulsive acceleration (Lin et al., 1973). The observed starting frequencies range up to 500 MHz, corresponding to plasma frequencies at densities up to 10^9 cm^{-3}. Most Type III bursts are unaccompanied by flares or soft X-ray bursts; hard X-ray emission occurs in coincidence with some flare-associated Type III bursts (Anderson and Winckler, 1962), especially those with high starting frequencies. Figure 4.1 (Kane, 1972) shows an example with coincident time structure; the X-ray and radio bursts are closely simultaneous. Note that the time scale for Type III's is in the range 0.1—1 sec.

Many Type III bursts begin at low frequencies, below 100 MHz, implying starting heights of > 1 R_0 above the photosphere. Further, many electron events are observed at 1 A.U. with spectra extending smoothly to a few keV (Potter et al., 1980) indicating that the electrons were accelerated > 0.5 R_0 above the photosphere.

Interplanetary measurements show that the spectrum of the escaping electrons is approximately a power law with index about 4 (Lin, 1974). The total number of

electrons at 1 A.U. from a typical event (group of bursts) is about N(> 5 keV) = 5 × 10³⁴. Many more fast electrons may be present near the sun since there may be substantial losses to the fast electron beam-plasma instabilities that are responsible for the Type III radio emission (see Smith, 1974).

This number and the knowledge of the density obtained from the radio burst enables us to estimate the minimum X-ray flux as a function of time:

$$dj/dh\nu_{min} = 2.5 \times 10^3(1 + 0.72t)^{-2.38}h\nu^{-4.5}ph/cm^2 \, s \, keV$$

giving a time-integrated X-ray fluence of ~4 cm⁻² for > 5 keV. Figure 4.2 shows the calculated P/OF sensitivity for bursts of this type, indicating that X-ray observations can be obtained over a range of heights in the corona comparable to those now achieved by radio observations.
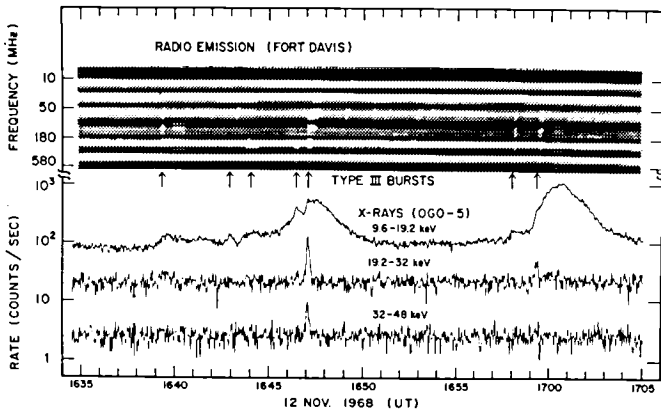

Figure 4.1—An example of the temporal correlation between impulsive solar > 10 keV X-ray bursts and type III solar radio bursts in the 10—580 MHz range.

Meter-wave radio bursts of Types V and U have a family relationship with Type III bursts, and probably share the same acceleration mechanism. In a U burst, the frequency decreases as in a Type III burst, but then increases in a fairly symmetrical manner. The natural interpretation is that the U burst acceleration took place in a closed flux tube, and that the electrons remained trapped as they streamed coherently up on one leg and down the other. Type V bursts follow groups of III's and appear again to come from the coronal trapping of clouds of electrons accelerated upwards. The calculation above refers equally well to the electrons that produce radio bursts of Types III, V and U.

With the unique P/OF ensemble of hard X-ray, white light, and EUV measurements we will answer the

following questions:

— *Where is the acceleration region located?*

— *How do the electrons propagate through the corona?*

— *What are the characteristics of the acceleration region, i.e., n_e, n_i, T_e, T_i, bulk flow and nonthermal velocities, etc.?*

— *Are there unusually high wave/turbulence levels in the acceleration region?*

— *What is the magnetic field strength and topology in the acceleration region?*

— *Are there flows in the acceleration region consistent with magnetic merging?*

— *How does the coronal structure change after a Type III burst?*

— *Do the electrons lose substantial amounts of energy in propagating through the corona?*
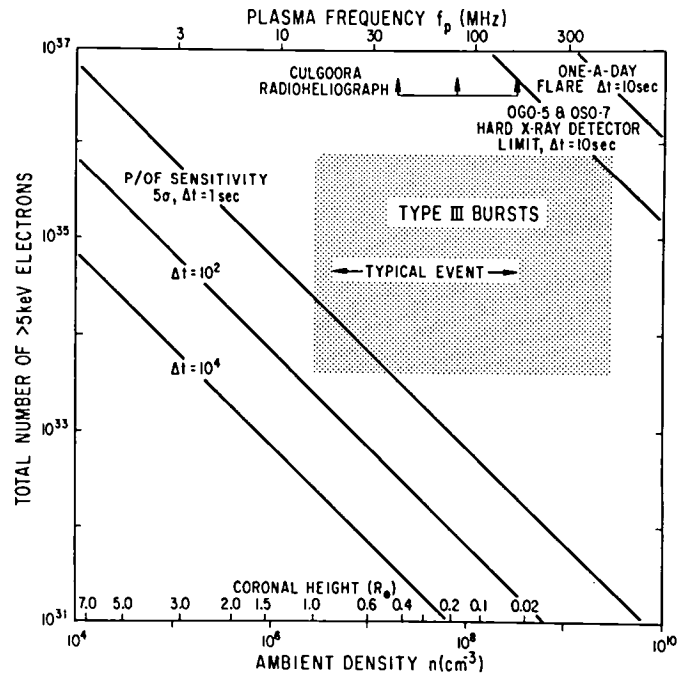

Figure 4.2—The 5 σ sensitivity of P/OF for detecting energetic electrons in the corona as a function of ambient density or coronal height (diagonal lines at lower left) is compared here with the sensitivity of typical full-sun hard X-ray detectors flown previously (upper right). For reference, the expected range of X-ray emission from type III bursts in once-a-day flares is shown.

4-2

4.3 Type II, Type IV and Flare Continuum

Major solar events commonly produce great disturbances in the outer corona, in addition to the impulsive phase/gradual phase phenomena in the chromosphere and low corona. Various manifestations of these disturbances include type II bursts, thought to be induced by the passage of a large-scale MHD shock wave outward from the flare, and type IV bursts of various kinds. Certain stationary type IV bursts are called "flare continuum" or FC sources, with the FC II type following a type II burst directly (Robinson and Smerd, 1975).

The hard X-ray data on sources related to these includes three examples isolated in the corona due to fortuitous occultation by the limb of the sun. These strikingly similar events were 1969 March 30 (Frost and Dennis, 1971), 1971 December 14 (Hudson, 1978), and 1972 July 22 (Hudson, *et al.*, 1981). Klein *et al.* (1982) have also reported a series of hard X-ray and meter-wave observations of flares on the visible hemisphere, concluding that extended hard X-ray emission is associated with moving type IV bursts, rather than stationary type IV's.

The 1972 July 22 event has been analyzed in detail in terms of its relationship with Type II, Type III, and FC II bursts, plus the observations of interplanetary particles (Hudson *et al.*, 1982). The hard X-radiation from each of these events lasted for almost an hour and displayed an extremely flat spectrum (power law index ~2.0); in each case this gradual coronal component of hard X-ray emission followed the impulsive phase by an appreciable interval. In one case (1971 December 14), a white-light coronal transient of the compact blob type was also observed (Brueckner, 1974).

We show in Figure 4.3 the height-time plot for the event of 1972 July 22. The clusters of Type III bursts mark the time of the impulsive phase initiating the Type II exciter; the gradual hard X-radiation closely matched the passage of the exciter past the 80 MHz plasma frequency height where Culgoora observations showed the FC II source. The interplanetary electrons were injected at approximately the same time, and produced the spectrum shown in Figure 4.4. We draw the following conclusions from the analysis of this event:

— The X-ray emission occurred at a density $\sim 10^8$ cm^{-3} and a magnetic field strength ~ 10 G.

— Acceleration was widespread and continued for tens of minutes.

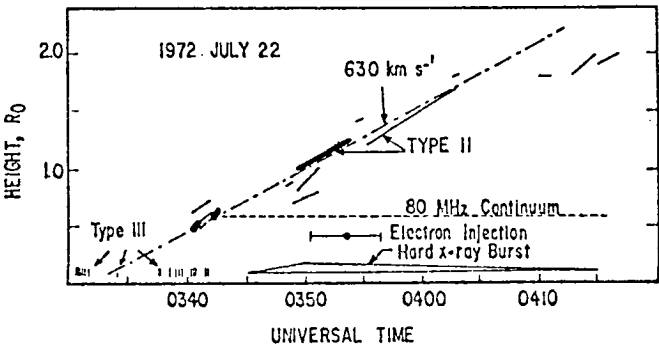— The accelerating agent was probably the shock wave that caused the Type II burst.

Figure 4.3—Height-time plot of the type II burst of 22 June 1972. Heavy sloping lines indicate type II bands assumed to be fundamental, while medium sloping lines represent assumed second harmonic bands. Also shown are the times of type III bursts (vertical bars), the flare continuum source at 80 MHz at an observed height ≈ 0.6 R$_0$ and the time profile of the hard X-ray burst.

Acceleration events of this type can easily be detected by sensitive P/OF observations. Some of the significant questions which could be answered for Type II burst acceleration are:

— *Does the particle acceleration occur where the magnetic field is nearly tangent to the shock surface as observed for shocks in the interplanetary medium?*

— *Or is the acceleration primarily a Fermi type?*

— *If a Fermi-type acceleration, is it a first-order Fermi acceleration at the shock, or between the shock and a magnetic loop (Wild et al., 1963)?*

— *Or is it a second-order Fermi acceleration involving turbulence behind and/or in front of the shock (Ramaty et al., 1980)?*

— *What are the conditions, i.e., density and temperature, in the acceleration region?*

— *Is this type of acceleration a second phase which requires an injection of pre-accelerated particles?*
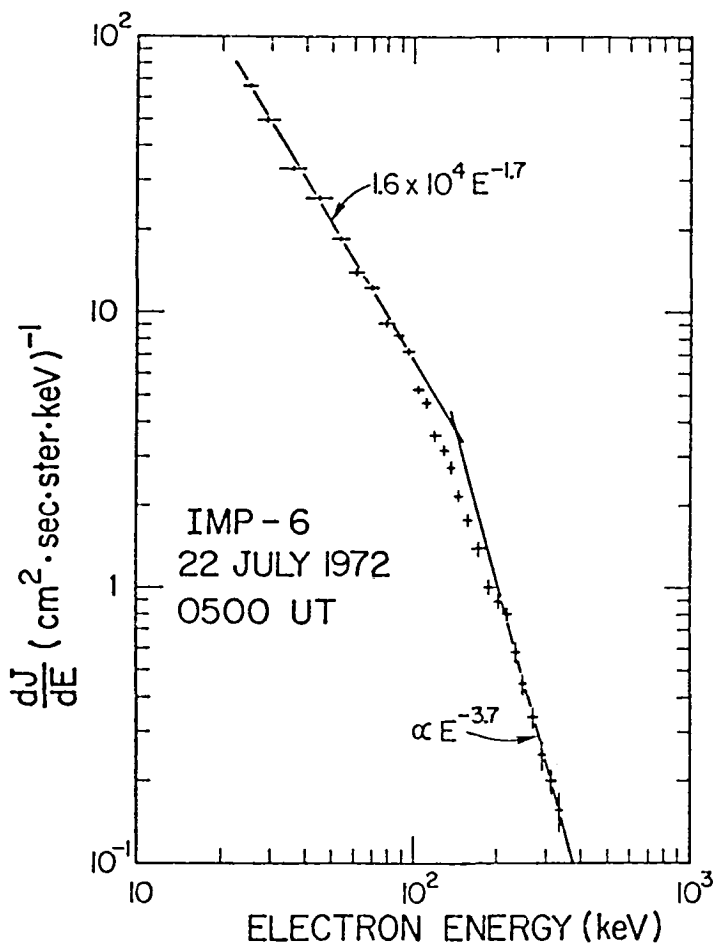
Figure 4.4—Spectrum of interplanetary electrons from the burst of Figure 4.3. The high- and low-energy asymptotic power law fits are shown; typically the high-energy power law extends to several MeV.

were not detected. In the observation, the source exhibits a remarkable constancy of temperature, implying a continued energy input perhaps associated with the nonthermal processes responsible for the radio emission.
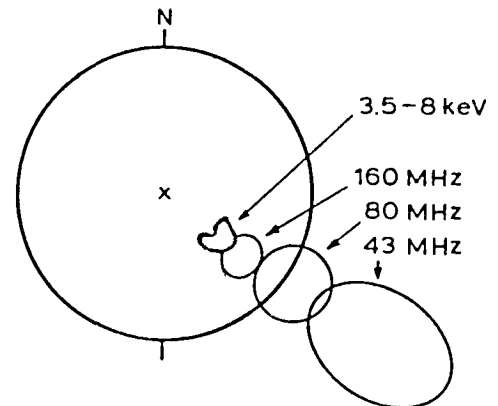

Figure 4.5—Giant arch observed in soft X-radiation following the flare of 1980 May 21. The radio observations of a type I noise storm indicate a close association with the X-ray source.

4.4 Type I Noise Storms

These most common of meter-wave radio bursts appear predominant in the vicinity of solar active regions. Type I noise storms often last for many days. They consist of both continuum and Type III-like bursts with frequency drift rates slower than III's. Recently (Webb and Kundu, 1978; Lantos *et al.*, 1981; Svestka *et al.*, 1982a,b) long-enduring soft X-ray sources with remarkable properties have been identified with type I noise storms following major solar flares. The X-ray sources of the 1980 May 21 event, Figure 4.5, appear to consist of enormous loop structures, lasting for many hours without any marked temperature variations; the line and continuum spectrum suggest an essentially thermal source. Since the radio burst did not coincide precisely with the X-ray source, it is probable that the nonthermal electrons responsible for the radio emission

Other examples of associations between the type I emission and soft X-radiation were found by Webb and Kundu (1978). Observations with high sensitivity, as provided by P/OF, are needed to observe the nonthermal electrons and thus to clarify the physics of heating and radio emission. Again the visible/UV coronagraph and the ultraviolet coronagraph-spectrometer will provide detailed diagnostics on the structure and conditions in the acceleration region.

The P/OF instrument complement provides an ideal source of measurements with which to answer some of the important questions raised by the initial observations:

— *What is the X-ray spectrum emitted by the actual type I region itself?*

— *What is the nature of the coupling between the coronal sources and the chromospheric variations?*

— *What is the distribution function of the electrons responsible for the type I radio emission?*

— *What is the topology of the magnetic field structures involved in these sources, and how does it relate to the filament and its motions?*

4.5 Second-Stage and Second-Step Acceleration

Our knowledge of high-energy particle acceleration by solar flares until recently came almost entirely from *in situ* measurements near or at the Earth. An abundance of γ-ray observations, especially from the Solar Maximum Mission (Chupp, 1981) has now given us a fairly direct view of the high-energy protons in the flare proper; this information parallels that derived from the hard X-ray spectrum.

The general characteristics of high-energy particles observed in interplanetary space strongly suggests a close connection with the shock disturbances known to propagate there (*e.g.* Hundhausen, 1972). This led to the concept of the "second-stage" acceleration, delayed considerably from the time of the flare impulsive phase. There is little doubt that such delayed acceleration does take place, both near the sun (*e.g.* the electrons accelerated in the Type II burst disturbance) and in deep space. However, as something of a surprise, the SMM data showed that the bulk of prompt γ-ray line emission occurs *during the impulsive phase*. This means that acceleration to high energies must take place rapidly (in a few seconds) and have a close connection with the impulsive-phase energy release.

Bai (1982) has described this new insight into particle acceleration by solar flares. He has found a slight delay between the impulsive phase ($\leq$ 50 keV electrons) and the high-energy protons and electrons. This delay always appears in γ-ray line flares (Bai *et al.*, 1982) *i.e.* those that succeed in prompt acceleration of protons. Furthermore, the delay appears to increase (from seconds to tens of seconds) as the spatial scale of the flare increases or as the duration of the γ-ray line emission increases (Gardner *et al.*, 1981).

The "second-step" acceleration appears, from these clues, to take place in the compact loops of the flare impulsive phase. The impulsive-phase acceleration serves as an injection mechanism, and then the shock disturbance causes further acceleration to high energies by a first-order Fermi mechanism. The Pinhole/Occulter Facility observations will allow us to determine the exact location of the second-step acceleration process, and to watch it evolve in time as the shock-wave propagates through the magnetic structures in the low corona. The full diagnostic information available from the white-light and EUV telescopes will give quite specific information about the physical conditions during the particle acceleration, and will identify what mechanism is at

work. It will be particularly interesting if these observations can provide some information about the nature of the turbulence required for particle scattering in the first-order Fermi process with a single shock disturbance.

Pinhole/Occulter observations will answer the following important questions:

— *Is the "second-step" emission co-spatial with the impulsive phase?*

— *Does the "second-step" excitation propagate with a shock disturbance?*

— *Or does the spatial dependence require a relaxation from an initial impulsive excitation?*

— *In the case of "second-stage" acceleration at a site removed from the flare proper, what are the physical conditions at the acceleration site?*

— *What triggers the onset of "second-stage" acceleration?*

4.6 Coronal hard X-ray sources

Stereoscopic solar viewing by two hard X-ray instruments (ISEE-3 and Pioneer Venus Orbiter) has given a valuable additional channel for deriving information about the spatial extent of solar hard X-rays (Kane *et al.*, 1982), and have shown fairly directly for a single event (Nov. 5, 1979) that the source of a gradual component of hard X-ray emission may have an appreciably greater height than the impulsive-phase sources. We show this result in Figure 4.6. Earlier observations of limb-occulted gradual hard X-ray sources (Hudson *et al.*, 1982) showed that the coronal sources of very hard spectra may extend quite high ($\geq$25,000 km) into the corona. This latter observation has been reinforced by more direct imaging observations from *Hinotori*. Figure 4.7 shows a large nonthermal source above a major Hα flare. Its loop shape suggests altitudes exceeding 50,000 km.

Finally, there is now evidence that the phenomena of solar flares can occur *wholly in the corona* without participation of the cooler layers of the atmosphere. The Solar Maximum Mission observed an extraordinary sequence of flare-like phenomena following an otherwise ordinary major flare on 1980 November 6. A regular series of events (Figure 4.8) produced hard X-rays, soft X-rays and transition region emissions in approximately

the normal proportions, but without Hα emission. This discovery implies that the flare instability with all of its subordinate mechanisms — particle acceleration, heating, "evaporation" and conduction, etc., can take place without involving the chromosphere in an energetically significant way.

Additional evidence for the occurrence of particle acceleration high in the corona is given by the discovery of electron events originating high in the corona (Potter *et al.*, 1981). These strongly resemble the type III bursts often associated directly with the flare impulsive phase.
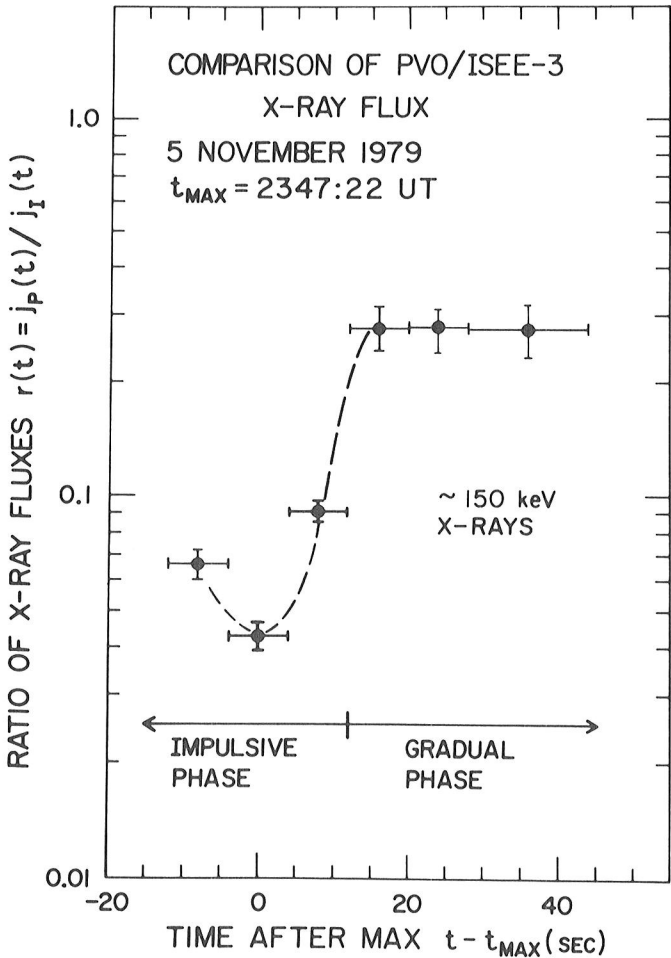

Figure 4.6—Ratio of fluxes observed by ISEE-3 and PVO detectors located near Earth and Venus respectively and thus at different solar longitudes. The variation of the ratio shows a varying fraction of occultation by the solar limb. The gradual phase appears to be *less* occulted, implying a greater vertical extent.

4.7 Observational Requirements

The detailed requirements for both X-ray and coronagraphic observations appear in sections 2.7 and 3.3, respectively. The considerations involved in determining these requirements included the prospect of faint

coronal sources, with the resulting need for great sensitivity. Many of the coronal particle-acceleration phenomena occur very commonly (*e.g.* type I and type III emission), so a Shuttle sortie flight will produce observations of many such sources. Others (moving type IV bursts, for example) occur less frequently, so that observations over a period extending as long as possible will eventually be required.

Figure 4.7—*Hinotori* observations of a hard (17-40 keV) source in the corona near a 3B flare of 1981 May 13, 0415 UT. The hard X-ray source appears near the loop prominence system, seen here as a set of H-alpha loops starting from the lower left (S) ribbon (Tsuneta *et al.*, 1982).
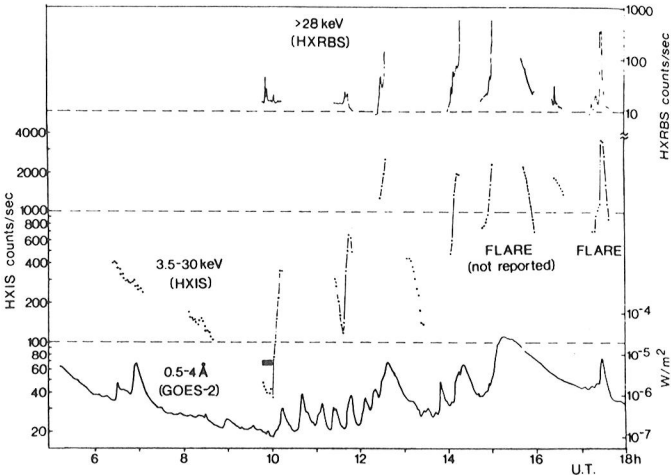

Figure 4.8—SMM observations of coronal activity following a major flare on 1980 Nov 6. These phenomena included many of the components of normal flares—in particular both hard and soft X-rays—but little trace of Hα or other phenomena of the chromosphere (Svestka *et al.*, 1982b).

5. Cosmic X-Ray Observations

5.1 Introduction

The hard X-ray imaging instruments of the Pinhole/Occulter Facility (*i.e.,* the coded aperture imaging and Fourier transform X-ray instruments) are extremely powerful tools for X-ray astronomy. Together they provide a more advanced capability for the hard X-ray portion of the spectrum than any yet flown. Sensitivity to point sources will permit determination of source fluxes, monitoring of variability, and measurement of spectra at levels an order of magnitude fainter than what has previously been available at these energies.

The Pinhole/Occulter Facility will improve sensitivity by at least a factor of ten for the traditional areas of hard X-ray astronomical investigation: spectroscopy and rapid variability of stellar sources with hard X-ray spectral components, including cyclotron lines and pulse phase spectroscopy in pulsars, and spectral/temporal variations of active galactic nuclei. Source classes near the sensitivity threshold of earlier instrumentation will be seen at high statistical significance. P/OF's high sensitivity and fine angular resolution give a mapping capability for extended components of active galactic nuclei and synchrotron nebulae such as the Crab Nebula, and also permit source spectra to be measured in regions of high source density such as the galactic center, the Magellanic Clouds, and M31. It will be possible to do deep integrations in order to determine the spectra and luminosity functions of various source populations at low flux levels and their contributions to the diffuse background in hard X-ray energies. A number of the cosmic X-ray problems on which P/OF can be used overlap with the solar issues described in the earlier chapters.

The sensitivity, angular resolution and wide range of purposes for which it is useful make P/OF the hard X-ray counterpart to AXAF. In this chapter we first explain P/OF's role and place relative to other X-ray astronomical observatories and facilities, flown or planned (section 5.2), and then describe specific scientific goals. Because the scientific applications are so diverse it has been convenient to group them according to the way in which they utilize P/OF: some draw upon its imaging to map extended sources (5.3), some utilize its high sensitivity for spectral and timing measurements (5.4), and some utilize the high angular resolution to resolve crowded source fields (5.5). Finally, the effect of P/OF on development of the link between solar and stellar astrophysics is discussed (5.6). In each of these areas P/OF should make major contributions to the advance of X-ray astronomy.

5.2 P/OF's Place Among Astronomical Facilities

The requirements of P/OF's Fourier transform (FT) and coded aperture (CAI) transform telescopes are summarized in sections 2.7 and 2.8. The two instruments contribute complementary capabilities for X-ray astronomy. The CAI instrument covers the larger angular size scales (8 arc sec to 17 arc min) and has greater sensitivity but a narrower energy range (2—35 keV). The FT instrument reaches finer angular scales (0.2 arc sec) and has a smaller field of view. It is also capable of imaging up to 120 keV. It is less sensitive, primarily because its masks require more opaque area (25% *vs.* 50% open area), and because more total detector area is devoted to the CAI design. The CAI and FT telescopes can be characterized as providing, together, imaging over angular scales from 0.2 arc sec to 17 arc min, at energies from 2—120 keV, with a point source sensitivity down to 0.03 μJy at 5 keV in 10^4 s.

We have analyzed the expected performance of both instruments, using both analytical estimates and Monte Carlo numerical simulations. We summarize here some results pertinent to X-ray astronomy and compare them with other X-ray instruments from HEAO-1 and the *Einstein* Observatory. The minimum detectable flux is found to be (where detector background >> diffuse background >> source total count)

$$F_{min} = 2\eta(\frac{B}{\epsilon A\delta E\delta t})^{1/2}$$

for an energy band δE keV and an integration time δt sec. We assume a 5σ detection significance ($\eta = 5$) and a background rate, B, of 3×10^{-4} cts (cm^2 sec keV)$^{-1}$ and an efficiency $\epsilon \sim 0.8$. The total geometric collecting area is 1.2 square meters and the effective area is taken to be 0.8 m^2. In a typical case (2—10 keV, 10^4 s integration) we find

$$F = 0.03 (\delta t/10^4)^{-1/2} \mu Jy$$

at 5 keV. (This is about 0.03 UFU.) Even very short integrations permit sources at 1 UFU to be seen. For harder X-rays (15—30 keV) the minimum flux detectable in a longer integration (10^5 s) is

$$F = 1.3 \times 10^{-5} \text{ cts / cm}^2 s$$

We can put these sensitivities in perspective by comparing them with those of other recent instruments and with

those foreseen in the future in Figure 5.1.

The comparison with HEAO A-2 demonstrates that P/OF will provide roughly an order of magnitude jump in hard X-ray sensitivity. The *Einstein* Observatory's HRI (High Resolution Imager) is the appropriate focal plane instrument with which to make comparison, since it is the member of that Observatory's complement which most nearly approached P/OF's angular resolution. (The HRI had angular resolution comparable to that of P/OF's CAI instrument; the FT telescope on P/OF is an order of magnitude better in angular resolution, but is less sensitive than the CAI instrument.)
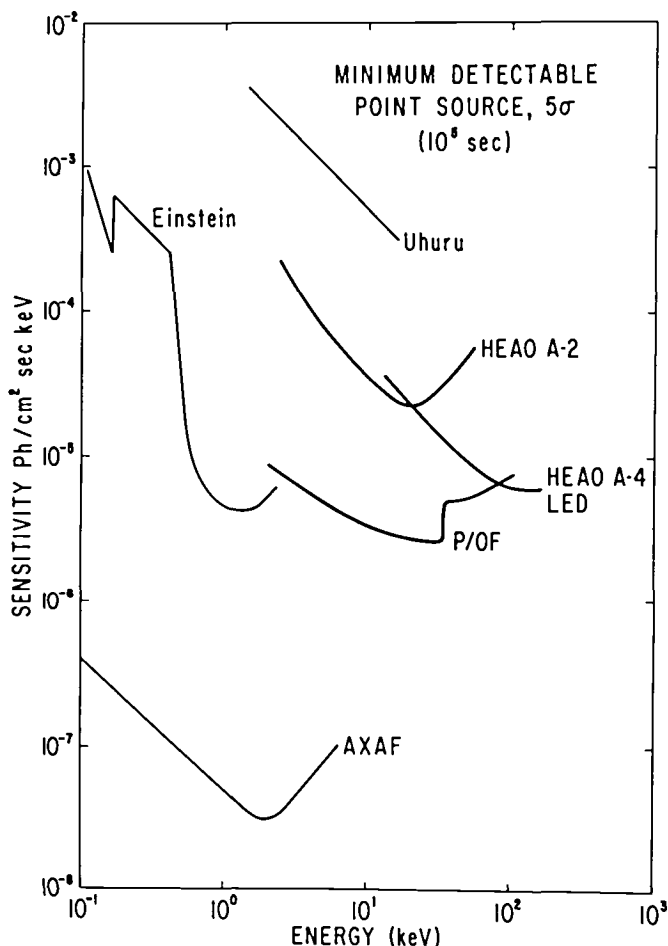

Figure 5.1—Sensitivity of the P/OF compared to recent (Uhuru, 1970; HEAO-1, 1977; Einstein, 1978) and planned (AXAF, 1990?) X-ray observatories. P/OF will provide a logical extension to the proven Einstein-range wealth of astrophysical information, and will provide complementary coverage beyond the range of AXAF, at reduced sensitivity.

Figure 5.1 shows that P/OF has roughly the sensitivity of the HRI. The HRI has an effective area of ~ 20 cm^2, but it has the full advantage of focusing, while the P/OF has a 1.5 m^2 unfocused area. The sensitivities are comparable, and this is clearly an important point, in

view of the enormous astronomical capability demonstrated by the *Einstein* Observatory (Giacconi *et al.*, 1979).

P/OF will not equal AXAF (the Advanced X-ray Astronomy Facility) in sensitivity. However, it will provide *complementary coverage at higher energies, and at roughly the same angular resolution*. P/OF's energy range overlaps with AXAF, from 2—8 keV, so that spectra from the two instruments could be merged. P/OF's role will be that of the hard X-ray counterpart to AXAF. This complementary role underlies much of the subsequent discussion of scientific objectives.

It is noteworthy that the limitation on P/OF's angular resolution for astronomical purposes (0.2 arc sec) is dictated primarily by the star trackers, rather than by the position-sensing X-ray detectors or by diffraction effects. There remains potential in the P/OF design to go to still finer angular resolutions in subsequent instruments. In this sense P/OF may be regarded as having an important engineering role, as a necessary developmental stage in evolution of yet more advanced instruments. Nevertheless, P/OF itself achieves angular resolution comparable to that of AXAF, Space Telescope, and the VLA in other wavelengths.

5.3 Scientific Objectives I: Hard X-ray Imaging

We begin with applications which utilize P/OF in its unique capacity as a high-resolution hard X-ray imaging instrument. Much of what it will see must be estimated by extrapolation from current knowledge of various source classes. P/OF has been optimized for compact sources of high surface brightness, and the mapping of these sources has barely begun.

5.3.1 Active Galactic Nuclei (AGNs)

The study of active galactic nuclei (a general category taken to include quasars, BL Lacertae objects, Seyfert galaxies, N-galaxies and emission line galaxies) is one where P/OF's imaging capabilities will provide a major new type of information on sources of fundamental importance to astrophysics. The bright, variable cores of galaxies are now recognized as a class of X-ray emitters whose total numbers and range of luminosities far exceed those of clusters of galaxies. From X-ray data there appears to be a nearly continuous range of X-ray luminosities extending from galaxies with narrow emission lines (about 10^{42} erg s^{-1}) through Type I Seyferts (10^{42}–10^{45} erg s^{-1}), N-galaxies (10^{45}–10^{47} erg s^{-1}), to

QSO's and BL Lacertae objects (10^{43}–10^{47} erg s^{-1}). In some cases a significant fraction of the total power radiated by the object appears in hard X-rays and gamma rays. The short timescales of variability of many of these objects (from hours to weeks) imply highly compact sources of emission in the very core of the galactic nucleus. For some time it has been suggested that the central power supply is the accretion of matter onto a massive (10^6–10^8 M_o) black hole. Optical rotation curves and photometry in M87 (Young et al., 1978; Sargent et al., 1978) lend support to this idea, although anisotropic velocity dispersions may fit the data without requiring a massive black hole (Duncan and Wheeler, 1980). X-ray observations from the Einstein Observatory strongly suggest that this phenomenon may be a common property of galaxies.

In addition to central cores of high activity in AGNs, X-ray jets have been observed in NGC 5128 (Cen A) extending from the core out toward the NE inner radio lobe. Figure 5.2 (Feigelson et al., 1982) shows Einstein Observatory images of the object. It has subsequently been shown that the jet includes small knots of synchrotron emission. The X-ray jet is strong evidence of the continuous flow of energy from the nucleus to the inner radio lobes and by extrapolation suggests how giant radio lobes seen in radio galaxies may be formed. Since the total energies estimated for giant radio lobes may reach as high as 10^{61} ergs (= 10^7 $M_o c^2$), a large fraction of the lifetime output of many AGNs needs to be ejected anisotropically, perhaps through jets.

P/OF is useful for studying structures in the form of jets. Angular scales seen in jets in 3C273, M87, and Cen A range from a few arc sec to several arc minutes. The jet in Cen A has an intensity of 3 x 10^{-12} erg cm^{-2} s^{-1}, or ~ 0.1 μJy, well above P/OF's threshold. The spectrum of the jet should be measurable from P/OF observations, something which was not possible with Einstein. Spectra of jets can also be isolated from other components of the active nucleus.

Moreover, we must be seeing with the Einstein IPC the largest jets from the nearest objects, i.e., the tip of the distribution. The number accessible to P/OF with its finer angular resolution should be far larger. The jet seen in Cen A is 4 arc min long and would occupy 200 pixels in the CAI. If this source were removed to a distance 10 times greater, it would be 25 arc sec long. It would still have the same surface brightness as it has at its actual distance, so that it could still be detected and resolved with P/OF were it at this greater distance. Consequently, P/OF will be able to inspect sources
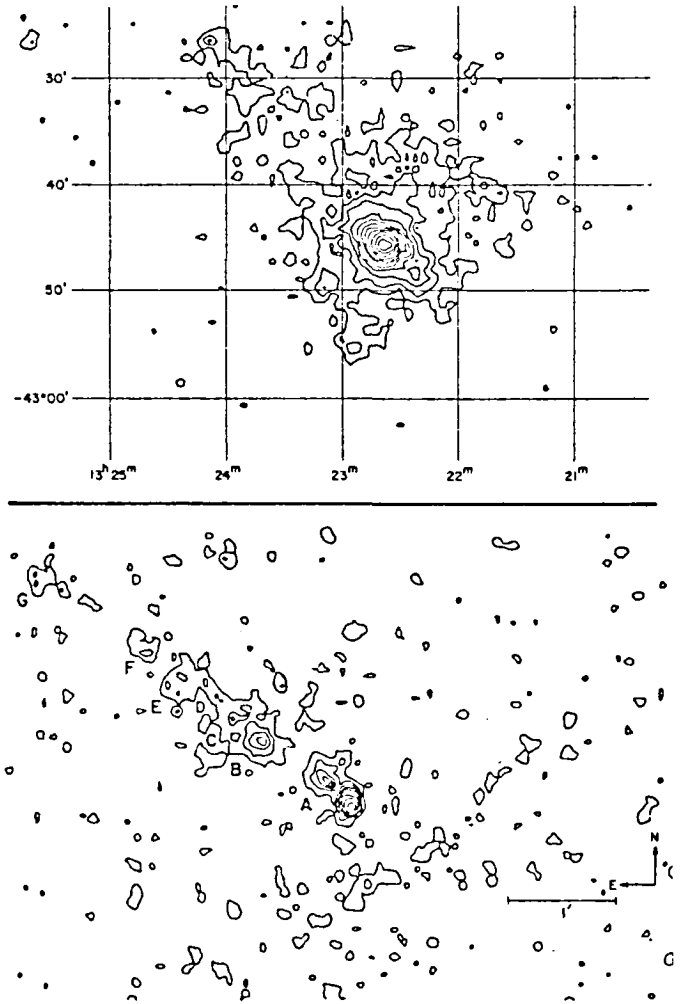

Figure 5.2—Einstein maps of Cen A. Top, contour map of the IPC image with 48" resolution. The first seven contours are 2 σ increments over an arbitrary zero level, while the higher contours are logarithmically spaced to avoid crowding. Bottom, maximum-entropy deconvolution of the central region of the HRI image, with 3" resolution.

within a volume 1000 times larger than that which was accessible to the Einstein IPC for jets like the one in Cen A. It is likely that source structures on smaller intrinsic scales will also be discovered. Radio counterparts of X-ray emitting AGNs have structures on many angular size scales, and there is increasing evidence of correspondence between radio and X-ray structure.

Relativistic motions are sometimes seen in AGNs, wherein observed structures change over the course of time. Sometimes the changes of structure observed at radio wavelengths appear to be supra-relativistic (i.e., if the linear distance traveled by a moving object is estimated by using the distance scale determined from the redshift, then the apparent velocity exceeds c). This paradox can be removed, but highly relativistic velocities are still required. Evidence of relativistic motion also

comes from attempts to reconcile hard X-ray observations of spectra and temporal variations with observations at lower energies. In these cases the rapid motions are not seen directly but rather are inferred from the need to prevent an inverse Compton catastrophe in the emission models. In the light of these considerations it will not be surprising to find that relativistic ejections have produced a variety of observable angular structures in the AGNs. It may be possible to observe temporal change in structures directly, in nearby sources such as M87.

Study of jets, relativistic motions, and extended structures in AGNs will undoubtedly assume great importance as sub-arc sec measurements in X-ray, optical, and radio wavelengths become available for comparison. We note that the galactic object SS433 exhibits jet structure also observed by *Einstein* (Seward *et al.,* 1981).

5.3.2 The Crab Nebula and Other Synchrotron Nebulae

The Crab Nebula and its pulsar are the remnants of the supernova of 1054 AD. Observations range from long-wavelength radio waves to the highest detected gamma-ray energies. Studies of the electromagnetic radiation from the nebula reveal that the nebular emission consists largely of synchrotron emission from high-energy charged particles moving in a magnetic field. This has focused attention on supernovae and their remnants as sources of cosmic rays. The structure of the high-energy emission leads one to the conclusion that the pulsar is the accelerator of the relativistic electrons in the nebula (Goldreich and Julian 1969). The pulsar rotation rate of 30 revolutions per second can only be achieved by a neutron star, an object of about one solar mass compressed to a diameter of order 20 km with mean density of approximately 10^{14} g/cm^3. The Crab Nebula and pulsar have become a Rosetta Stone to astronomers, revealing in one object many extreme physical conditions: million-degree temperatures, relativistic gases, regions of extremely high matter densities, and high-magnetic and gravitational fields. Physical insights gained from the Crab are often transferable to other astrophysical situations. For these reasons, the Crab will be a major target for P/OF observations. We show the Crab Nebula in Figure 5.3 including recent hard X-ray observations.

P/OF is the only facility capable of studying fine-scale details of the transport process of the relativistic electrons away from the pulsar as a function of energy.
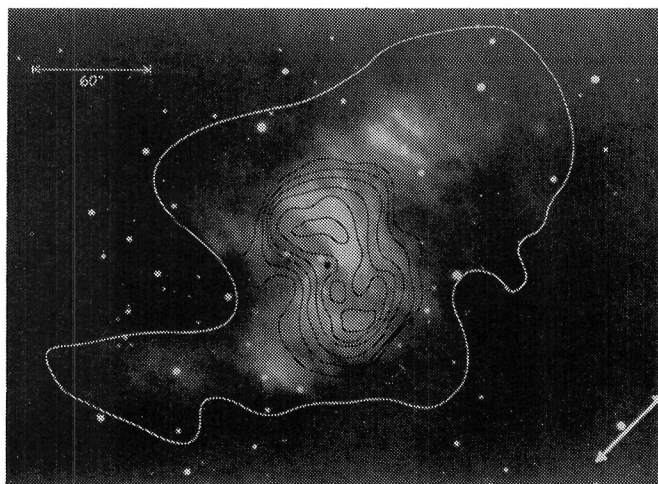

Figure 5.3—Crab Nebula: the bright synchrotron emission region is shown with hard X-ray (22-67 keV) contours superimposed. The hard X-ray nebula is about 60 arc sec long and 30 arc sec broad (FWHM). The X-ray contours are synthesized from linear scan data with a limiting resolution of ≈ 15 arc sec. Higher resolution X-ray observations should reveal finer structure which would directly relate to the energy transfer processes occurring between the pulsar and the nebula. Optical image from Baade (1956).

A general picture of the energetics of the Crab has already been developed from lunar-occultation studies (Wolff and Novick, 1976). If diffusion predominates, the diameter of the nebula should decrease at higher energies. If there is bulk transport of plasma, the nebular size may either be insensitive to measured photon energy, or else may fall off with energy less rapidly than in diffusion models. With some good fortune the temporal behavior of the diffusion process can be explored as a function of energy and correlated with glitches in the pulsar spindown rate. The spindown glitches are related to substantial energy changes in the pulsar and may result in variations in the production of relativistic particles.

Although the Crab Nebula was one of the earliest extrasolar X-ray sources to be detected, it stood in a class by itself for ~ 15 years until the *Einstein* Observatory found other examples of nebulae, associated with pulsars or supernova remnants, in which synchrotron radiation appeared to be the emission mechanism (Becker *et al.,* 1982). Now that objects of this type begin to constitute a class, they can be arranged in sequence according to age, and the evolution of the injection rate of relativistic particles can be correlated with the decreasing spin of the pulsar. The cases where synchrotron nebulae are known or suspected include the Vela SNR, CTB 80, 3C58, and faint extended sources near a few of the known radio pulsars. It is important to

measure the spectra of these nebulae, both to determine whether they are nonthermal spectra and to compare with spectra from the associated pulsars, where those are available.

5.3.3 Other Supernova Remnants

Supernovae are among the most energetic phenomena observed in nature. They apparently convert nearly 10% of a solar mass into energy on a timescale of seconds. The bulk of this release ($\sim10^{53}$ ergs) probably appears as a burst of neutrinos, and possibly as gravitational radiation. A short pulse of X-rays lasting a few tens of seconds to minutes may accompany the passage of a shock wave through the outer envelope of the uncollapsed shell of the star prior to its expansion, carrying away some 10^{44} ergs. Ensuing expansion of the shell gives rise to the characteristic optical light curve. The expanding shell radiates most of its thermal energy in the visible band of the spectrum for a period of several months until expansion dilutes the gas to the point where its optically thin emission fades below the detection threshold. Extensive theoretical modeling of the supernova explosion has been carried out over the past several decades for a wide range of stellar masses and compositions. It appears from radio optical, and X-ray observations that supernovae may play an important role in cosmic ray acceleration, heating of the interstellar medium, and enrichment of the interstellar gas by heavy elements.

X-ray observations have revealed the line emission from highly ionized iron, neon, oxygen, silicon, sulfur, argon, and calcium atoms residing in the younger remnants. Surface-brightness maps generally show shell-like structure with a relatively sharp outer boundary. Young remnants are generally thought to be in an adiabatic phase of expansion, as they sweep up gas from the ambient interstellar medium, although the youngest remnants such as Cas A may be in transition between the piston expansion phase and the adiabatic phase (usually characterized as the point where the mass of swept-up interstellar gas equals the mass ejected in the initial explosion).

P/OF is best suited for studying the young, hot remnants by virtue of their higher surface brightness and temperature. In several ways these are the most interesting, since the amount of swept-up interstellar material is not large compared to the initial ejecta. The element mix contributed by the supernova dominates, and the basic question of how supernovae affect cosmic abundances can be examined. Through spectral and spatial studies we can deduce the elemental content and possibly something of the spatial distribution of the primary material ejected. The early development of turbulence in the piston-expansion phase, which leads to the thermalization of the material that was originally outflowing radially, is an interesting hydrodynamics problem, for which observational input from P/OF will be very helpful.

To make the discussion quantitative, consider the Cas A supernova remnant. The total flux from the remnant is 10^{-9} erg cm^{-2}s^{-1} in the 2—30 keV band. The surface area emitting at low energy based on the *Einstein* picture (Figure 5.4, from Murray et al. 1979) is about six square arc minutes. The flux per pixel is 4×10^{-12} erg cm^{-2} s^{-1} pixel^{-1}, where each pixel is ten arc sec on a side, yielding a good signal/noise ratio. Since the source spectrum falls off rapidly with energy compared to the detector internal background (E^{-3} vs. E^{-1}), mapping could be continued only up to about 10—15 keV. Other supernova remnants emit with lower surface brightness, but Tycho, Kepler, RCW 86, and RCW 103 are accessible to P/OF. Study of young supernova remnants in the Large and Small Magellanic Clouds is possible; a remnant such as Cas A would subtend 15 arc sec at the distance of the LMC.

Figure 5.4—Einstein HRI image of Cas A at high contrast. The ring-like structure is 4—5 arc min across, each pixel is 2"×2" and the exposure time is 32,519 sec (Murray et al. 1979). Detailed comparison of X-ray, optical and radio images show various degrees of correlation, indicating that several emission processes are present.

Temperature gradients and structure have been detected in several remnants, specifically SN1006 by Pye *et al.* (1981) and Cas A by Fabian *et al.* (1980). Gradients can alter the mixture of lines contributing to the X-ray spectrum. With the greater bandwidth available to P/OF, these gradients can be determined in substantially better detail, resulting in improved masses and chemical compositions.

5.3.4 Clusters of Galaxies

The X-ray surface brightness of clusters of galaxies has been studied extensively by the *Einstein* Observatory at energies below 4 keV. Most clusters emit at temperatures >4 keV, with typical temperatures being about 8 keV. Some are known to have spectra with tails extending to higher energies (Reichert 1982, Lea *et al.*, 1981), suggesting a nonthermal source superimposed on the emission from the intra-cluster gas that dominates at low energies. It is not known whether the hard spectral components are associated with the general emission from the cluster or with individual galaxies. Measurement of emission temperature from a thermal X-ray continuum requires detection of photon energies up to at least kT, as does the efficient observation of hot or nonthermal components in the presence of cooler ones.

There is also one very important spectral line feature in the energy range above 2 keV, the group of iron lines near 6.7 keV. In a thermal plasma of cosmic abundance at a temperature of a few keV, these are the only strong atomic lines emitted. The spectral feature is in fact a blend of lines from at least two ionization states, depending on physical conditions in the source. With a proportional counter only the total intensity of the feature and not the individual line strengths can be detected. In an optically thin plasma, the line intensity is a function of both temperature and iron abundance. If temperature can be determined from the X-ray continuum, then the iron abundance can be estimated. Determination of emission temperatures and gradients with continuum measurements above 4 keV and mapping of cluster iron lines (for surface brightnesses only 10% of the Coma cluster) will thus provide valuable diagnostics for the study of several important issues concerning clusters.

P/OF is ideally suited to detect and map the low-level inverse Compton emission expected from galaxy clusters in which diffuse radio emission is detected. This will appear as a nonthermal component superimposed on the thermal emission from the hot gas. It will thus be difficult to distinguish as a separate spectral component even with AXAF (with sensitivity only to ~ 8 keV) and will require high sensitivity imaging at hard X-ray energies.

A typical cluster has a low surface brightness, so that the angular resolution of P/OF is actually too fine for optimum sensitivity in most cases. However, regions of enhanced surface brightness (hot spots, regions of nonthermal emission, and compact objects) within the cluster, identified from earlier mappings, will readily be resolvable with P/OF. These hot points are clearly shown in range 0.1–3 keV. It would be surprising if there were not brighter small-scale features that would be ideal for P/OF's finer resolution, particularly in the vicinity of massive or active galaxies.

The morphology of the cluster X-ray emission can be related in a detailed way to the evolutionary stage of the cluster. A vital role in evolution of galaxies in the cluster is played by the intergalactic gas responsible for the X-ray emission. This gas presumably includes a primeval component, although according to present ideas it may not be a major component by mass. The gas is enriched by matter ejected from the galaxies when supernovae occur in them. Interstellar gas is also removed from galaxies by their motion through the cluster gas. The best means of distinguishing gas that has been stripped from the galaxies from primeval gas is provided by iron-line emission, since only the former type of gas will have undergone nuclear processing in stars. (There is also a possibility of producing iron-rich gas from supernova activity in a population of massive stars, prior to galaxy formation.)

Another interesting and important problem (which also has implications for the studies just discussed) is the state of mixing of the intra-cluster gas, and the transport of energy within it. At one extreme the gas may be well-mixed and characterized by an adiabatic temperature distribution. At the other extreme gravitational separation of heavy elements such as iron near the cluster center of mass can be envisaged. Maps of the iron feature and of the temperature distribution (determined from the slope of the X-ray continuum) will contribute to this problem.

Thus the high-energy, high angular resolution observations of clusters to be made with P/OF are complementary to those which have been or will be made at lower energies with instruments such as *Einstein* or AXAF. The close similarity in angular resolution of AXAF and P/OF is particularly important, and the sensitivity of P/OF, while lower than AXAF, is very good indeed and

will allow observations of a large number of objects to be made.

5.4 Scientific Objectives II: Photometry and Spectroscopy

Although some hard X-ray sources are resolvable now or will become so with P/OF, the greater part of X-ray astronomy involves point sources, many of them so exceedingly compact that they should remain unresolvable by any technique for the foreseeable future.

Among these point sources, there are many that contain high-temperature or hard nonthermal spectral components. A list currently would include pulsars, black hole candidates, bursters, degenerate dwarfs, RS CVn systems, flare stars, Seyfert galaxies, emission line galaxies, N galaxies, BL Lacertae objects, and quasars. These systems are all of central importance to high-energy astrophysics. In each case, current theoretical understanding is largely founded on and tested by means of observed spectra and temporal variability patterns. A special interest attaches to the hard X-ray measurements, either because the highest temperatures produced in the source are manifested there or because nonthermal components can be isolated in hard X-rays from thermal components or absorption effects. In addition the hard X-ray band happens to be where a number of important spectral features are encountered: iron lines, cyclotron features (emission or absorption), and breaks in nonthermal continuum spectra.

Thus, despite the diversity of masses, luminosities, spatial dimensions, and other physical parameters characterizing these sources, it is true of them collectively that further spectral measurements and timing studies in hard X-rays are vital to progress in understanding their physics, which often involves conditions or processes that cannot be studied in the laboratory. Outstanding problems include the role of cyclotron processes in pulsar radiation, the hard X-ray tails associated with shock heating or with Comptonization processes, the hard X-ray emission from stellar flares, and the evolution of spectra during outbursts in active galactic nuclei.

A few of the more important cases will be developed in this section. (RS CVn systems and flare stars will be deferred to section 5.6, in order to emphasize their connections to solar physics.) In each instance P/OF provides the best hard X-ray data base for the investigation of these sources because it has the best sensitivity of any instrument yet shown in the hard X-ray range, and because it has the position accuracy

necessary for unambiguous identification of sources responsible for outbursts and transient activity. This brief survey of hard X-ray astronomy does not attempt to be exhaustive, largely because these same two considerations tend to make P/OF the instrument of choice for a wide range of observations — especially any hard X-ray observation of a point source. In the applications in this section P/OF will be building upon and refining the understanding that has been built up from previous missions such as *Uhuru*, SAS-3, HEAO-1, and *Einstein*.

5.4.1 Binary Pulsars

Neutron stars accreting from binary companions have occupied a central place in X-ray astronomy ever since *Uhuru* observations of Hercules X-1 and Centaurus X-3 established the basic nature of these sources. The pulse period (which ranges from 69 ms to 10^3 s in the known cases) is associated with the neutron-star spin; longer periodicities are associated with orbital motion and with the motions of the accretion disk. In most of the $\sim$ 20 known systems, the spin period of the neutron star decreases over time, but this spin-up is irregular rather than steady, presumably because of the noisy character of the accretion torque. Variations in period and luminosity are the response of the star to the accretion torque and associated energy input, respectively. Infalling matter is funneled to magnetic poles by the magnetic field. The gravitational energy released in falling through the large potential drop to the stellar surface appears as pulsed radiation. The spectrum is typically very hard and in some cases exhibits cyclotron emission or absorption features.

The foregoing picture needs to be unified and completed in detail, answering questions concerning the nature and temporal structure of accretion flows, the internal structure of the neutron star as revealed in its dynamical response to the accretion torque, the range of intrinsic parameters of the neutron stars (primarily masses, moments of inertia, and magnetic moments), and details of the energy-conversion process responsible for the pulsed emission (including determination of the geometrical structure of the accretion column, of radiation mechanisms responsible for producing the pulse, and of the role of cyclotron processes in the accretion column and magnetosphere). Cyclotron processes are intrinsically associated with the strong (10^{12}–10^{13} G) magnetic field near the stellar surface. Electron energy levels are quantized in units of the cyclotron frequency (given by $h\nu_c = 11.6 \, B_{12}$ keV for a field strength $B_{12} \times 10^{12}$ gauss) and resonant transitions

exist, which may show up either as emission or absorption features. Features have been reported in Her X-1 (60 keV) and in 4U 0115+63 (20 keV), both within P/OF's range.

Future observations aimed at refining understanding will have to be subtle measurements, calling for high sensitivity, broad spectral coverage, and the ability to sample on appropriate timescales; this constitutes the program of the X-ray Timing Explorer. The measurements needed include (i) more detailed pulse-phase spectroscopy, (ii) observations of temporal variations in pulse profiles, down to the level of pulse-to-pulse variability, (iii) period fluctuation and luminosity-fluctuation measurements and (iv) observations of spectral features associated with cyclotron processes or iron emission. P/OF will provide all of these observations, and will have the ability to reach relatively faint sources.

Pulse-phase spectroscopy is useful in establishing details of the emitting-region geometry and the physics underlying the production of the pulse. As the star rotates one observes differing combinations of the effects of the angular distribution of radiation, spectral emissivity, and radiative transfer. The variability of the light curve provides further information, since it shows which features are rigid and which are subject to instabilities or are sensitive to fluctuations in the accretion flow. Those fluctuations can also be studied using the techniques proposed by Lamb, Boynton, and their collaborators (Lamb and Pines, 1979), in which the principal quantities observed are variations in the spin period, P, and the luminosity of the source, L. The Fourier transform of the time-varying accretion torque is expected to approximate a power law. Time variations in P and L can similarly be Fourier-transformed. The role of the neutron star can then be likened to that of a band-pass filter that responds differently to different frequencies. If the characteristic timescale for transfer of angular momentum from the crust to the core is T, then the star's response should be of higher magnitude at frequencies above $2\pi/T$ than at lower frequencies, because at the higher frequencies only the moment of inertia of the crust is involved, rather than that of the whole star. Observation of cyclotron features in the spectra of binary pulsars began with detection of such features in the spectrum of Her X-1 by Trumper et al. (1977). The features are observed to be time-variable. Cyclotron measurements establish the strength of the magnetic field in the magnetosphere and serve as a test for quantum-mechanical calculations of cross sections. Their dependence on pulse phase may provide a new way of studying radiative transfer in the magnetosphere.

5.4.2 Black Hole Candidates

Black holes, or gravitationally-collapsed regions, are predicted in most theories of gravitation, notably including General Relativity. If a mass M is confined within a region roughly the size of the Schwarzschild radius ($R_S = 2GM/c^2$), a "trapped surface" is formed, and only very limited information can subsequently be derived concerning what is inside that surface. When the black hole occurs in a binary system, it becomes a practical target for astronomical observations, by virtue of the mass it accretes from its companion. The accreting mass is deposited at the edge of an accretion disk and moves inward toward the black hole, becoming hotter and radiating as it does so.

Cygnus X-1 has been the leading black hole candidate in our own galaxy ever since the discovery that it is a compact object whose mass exceeds the probable upper mass limit ($\sim 3M_o$) for a neutron star. It exhibits rapid variability on short timescales (a few ms or shorter), presumably associated with energy release mechanisms in the accretion disk (Oda et al. 1971; Rothschild et al. 1974; Nolan et al. 1981). There is also a long-term switching between hard and soft spectral states. The distinctive temporal and spectral signatures are to a large extent duplicated in two other sources, Cir X-1 and GX 339-4. Mass determinations have not been made in these instances but they both show switching of spectral states and rapid variability, in the case of GX 339-4 on timescales as short as 50 ms. Similar rapid variability in that source has recently been seen in optical wavelengths (Motch et al. 1982).

Hard X-ray observations of black hole candidates are aimed at determining more about the rapid fluctuations and spectral switching, since these are the phenomena that are common to the small class of black hole candidates. It is important to establish how these effects are related to the physics of the accretion disk. The large area of P/OF can be used to isolate spectra of single outbursts, or to study their temporal structure.

5.4.3 Other Binary Systems

We briefly mention other kinds of binary systems that could be studied with P/OF. AM Herculis, a low-mass binary system made up of a dwarf M star and a magnetic degenerate dwarf, has a hard component that may represent Comptonized photons produced by shock-heated electrons. Flickering on short timescales has been seen, and there is a strong iron fluorescence line. Since AM Her is a rather faint source ($\sim 2 \mu Jy$ in

hard X-rays), P/OF will see it much better than earlier high energy instruments, and the hard X-ray component can be examined in detail. Hard X-ray components may be present in brighter binaries, such as Cyg X-2 or Sco X-1. Cyg X-2 is also interesting in another context, namely the unique temperature-luminosity signature reported by Branduardi et al. (1980). The luminosity sometimes varies roughly as T^4, but at other times the luminosity reaches a maximum value and then becomes insensitive to temperature. The latter conditions may represent times of extremely high mass accretion rate, according to the model proposed by Kylafis and Lamb (1979). Further study of the luminosity-temperature relationship is needed in Cyg X-2 and other sources to confirm the model.

5.4.4 Spectra and Variability of Active Galactic Nuclei

Extended structures in active galactic nuclei were discussed in 5.3.1. However, many components in AGNs have radio angular sizes on the order of a milli-arc sec, and there is reason to think some X-ray compact components will be at least that small. These compact components must be studied on the basis of spectral and temporal variations. It is known that spectral indices in hard X-rays vary somewhat with the type of AGN. Seyfert galaxies have spectral indices distributed over a narrow range (the photon number index is typically ~ 1.6). BL Lacertae objects sometimes show spectral breaks in hard X-rays.

Temporal variability is present in most of the objects on scales less than 1 year. There are also extreme cases of rapid variability. PKS 2155-304 is a BL Lacertae object that has the shortest timescales of any member of its class, being variable by a factor of two in six hours (Snyder et al., 1980). At the distance indicated by its reported redshift, this object has an X-ray luminosity of 10^{46} erg s^{-1}. NGC 6814 (Tennant et al., 1981), a low-luminosity Seyfert galaxy, and the quasar 1525+227 (Matilsky et al., 1982) are two AGNs that have been reported variable on timescales of 100 seconds.

Further spectral and temporal measurements are needed, especially in order to follow the evolution of the spectrum during outbursts. In this way it should be possible to distinguish, by watching what happens to spectral breaks as the burst evolves, whether outbursts decay radiatively or by adiabatic expansion of the source volume. It is also important to continue to establish the mean spectral index and its dispersion for each

of the various classes of AGNs in order to improve models for source emission regions as well as to make comparisons with the diffuse background.

5.5 Scientific Objectives III: Resolution of Crowded Fields

In some parts of the sky the field is sufficiently crowded that traditional detectors with fields of view of a few square degrees become source-confused, sometimes at flux levels as high as 20 μJy. Even a single bright source near a desired target can sometimes be a nuisance. Hard X-ray astronomy is then possible only to a limited degree, e.g., for studying bursts or periodic pulsations. At low flux levels (below about 0.5 μJy) this situation exists virtually everywhere in the sky, even for high-resolution collimators, because of the increase in the number of faint sources as the threshold is lowered. P/OF's imaging capability and high resolution remove these difficulties and open up a number of important avenues for new investigations.

5.5.1 The Galactic Center ("GCX")

The region of our galactic center shown in Figure 5.5 contains six X-ray sources within a region of only about one square degree (Skinner, 1979; Watson et
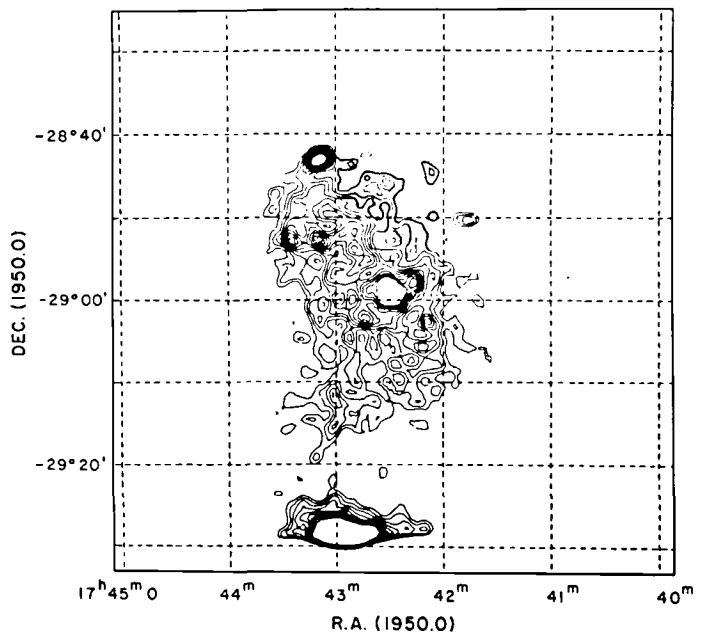

Figure 5.5—Maximum entropy deconvolution of Einstein IPC ($\approx$ 0.9–4 keV) images of the galactic center. The contour levels are linearly spaced. The width of the image is $\approx$ 60 arc min, and is dominated by a bright central region elongated along the galactic plane with total dimensions $\Delta l \times \Delta b = 25' \times 15'$. This region contains a number of unresolved "point" sources (Watson et al. 1981). The strong source at the bottom is A1742-294.

al. 1981). The interstellar absorption in this direction is severe, producing an X-ray cutoff at about 3 keV. The crowded field makes temporal studies ambiguous without the use of fine collimators or imaging. The spectral cutoff reduces the effectiveness of focusing-optics imaging systems, since the X-ray reflectivity of the mirror begins to fall off for most telescope designs by about 4 keV. The sensitivity of P/OF is nearly three orders of magnitude better than the current surveys above 4 keV and represents an important new capability for studying the region, which may well contain a black hole. There are three known X-ray bursters in this vicinity, which may be monitored simultaneously. There may be other surprises. Proctor *et al.* (1978) observed three X-ray bursts within six minutes from the GCX region, a number substantially larger than what would be anticipated on the basis of bursts seen in other parts of the galaxy. Finally, the hard X-ray imaging will certainly help to identify the sources of γ-ray emission (Matteson, 1982), including the 511 keV emission-line sources (Leventhal *et al.*, 1978).

5.5.2 Nearby Galaxies: LMC, SMC, M31

In addition to the distant powerful AGN sources, nearby galaxies such as M31, M33, and the Magellanic clouds can be imaged and their sources monitored for spectral and temporal variability. Eclipsing binaries and pulsating binaries can be discovered, increasing the number available for determination of neutron star masses. So far, masses up to 1.4 M_o have been discovered, but on theoretical grounds masses up to 3 M_o are allowed. X-ray burst sources will also be detectable in these external galaxies. It will also be possible to obtain a limited amount of spectral information on the brighter sources in the nearby galaxies. These may be the ones of greatest interest, especially if they have luminosities near or exceeding the Eddington limit for neutron stars, since they would necessarily be candidates for black holes. A source with luminosity 10^{40} erg s^{-1} could be seen at 5 Mpc. Several such $\sim 10^{39} - 10^{40}$ erg s^{-1} sources have been detected in nearby galaxies with *Einstein*, and P/OF could measure their spectra.

5.5.3 Faint Sources and the Diffuse Background

P/OF can be used in hard X-ray deep surveys to investigate source populations making up the hard X-ray sky at faint flux levels. This will help establish luminosity functions directly for those populations, and other parameters such as the mean ratio of X-ray to optical luminosity for complete X-ray selected samples. It may also turn up examples of sources at larger cosmological

distances than those currently known, and thereby help to determine the evolution of these populations. Every time P/OF does an integration of duration 10^4 s it may pick up a serendipitous source, and over the course of time the total number of these will grow large.

These source counts can then be used to estimate contributions to the diffuse background in hard X-rays. It is known from the *Einstein* Observatory results that quasars must contribute a large fraction of the soft background, but the possibility that a portion of it comes from other sources such as a hot intergalactic medium cannot yet be excluded. If such a hot gas exists, then it must constitute a large portion of the matter in the universe. Much improvement in the confidence placed in the conclusions reached is gained by working with sources at low flux levels, because these are the critical ones that must make up much of the background. Otherwise it is necessary to make assumptions in extrapolating the way in which flux ratios vary with absolute luminosity or with cosmological epoch. Furthermore, the hard X-ray diffuse background has its own particular feature of interest, a spectrum-steepening which occurs somewhere in the vicinity of 50–100 keV. If the diffuse background is dominated by the contributions of active galactic nuclei, primarily quasars, then there need to be quasars whose spectra break in this way. The best-determined quasar spectrum, that of 3C273, does not show such a break, but it is hardly a typical case. Spectra of a substantial sample of quasars would help address this question.

Ultimately, it would be possible to use P/OF to perform very long integrations sufficient to resolve the diffuse background. (P/OF will not become confusion limited in long integrations.) If the diffuse background is entirely composed of discrete sources, then it can in principle be resolved by long observations of a single region of the sky. For example, a composite diffuse background could consist of $\sim$ 300 sources per square degree, with the faintest and most numerous sources being at $\sim 10^{-9}$ Jy. From the sensitivity curve we see that this flux level could be reached in integrations of about 10^6 seconds. In reality, integrations would probably have to be somewhat longer than this, but even so they would surely be justified if they would firmly settle the question of whether the hard X-ray background has a diffuse component, a question that has remained controversial for more than a decade.

Long integrations and deep surveys would serve other purposes, for example, monitoring of variable AGNs over several days or searching for short-duration transients ($10–10^5$ s duration). Any transients found could

be positioned accurately and identified. From current understanding, it would be expected that many of these would turn out to be stellar flares. A determination of the morphology of these faint stellar flares would be quite informative.

5.6 Scientific Objectives IV: The Solar-Stellar Link

P/OF is the first large facility that would be suitable both for solar and cosmic X-ray observations. Thus it is especially fitting that it will encourage the development of links between solar and cosmic X-ray astrophysics at the scientific level, by providing data from which the extension of solar physics to analogous stellar physics can be undertaken.

Single stars and binaries made up of normal, nondegenerate stars have been observed in X-rays, including detections both of flares and of persistent emission. Stellar flares are bright enough to have been seen with fairly small proportional counters. The main sources of stellar flares are the RS CVn systems in close binaries in which optical light curves have for some time given a suggestion of the presence of "starspots" covering much of the star (Eaton and Hall, 1979). These are the most luminous nondegenerate stellar systems in X-rays, with luminosities of 10^{30}–10^{31} erg s^{-1}. Outbursts in which observed fluxes reach 50 UFU are known. In HEAO-1 observations it has been possible to track flaring activity through two successive flares from the same object, in hard X-rays. Flare stars (prototype UV Ceti) have been seen in X-rays (Heise et al. 1975) for several years. On one occasion it has been possible to monitor an event in X-ray, optical, and radio wavelengths (Kahler et al. 1982). W Ursae Majoris stars are another type of contact binary in which fluxes have been measured above 1 keV by HEAO-1; X-ray luminosities are 10^{30}–10^{31} erg s^{-1}, and intense UV lines have been seen with IUE. No flares from these objects have yet been reported.

Solar activity provides a good source of models for many forms of stellar activity (e.g. Rosner, 1982). The stellar data are useful in two ways. First, stellar coronal events may extend the dynamic range known from solar events. The largest known energy releases of this kind found in nature are provided by the stellar, not the solar, examples; X-ray flares as bright as 200 μJy have been seen from dMe stars. Second, there are theoretical questions in solar physics that can be addressed by examining stars over a wider range of spectral classes. For example, coronae have been seen with Einstein over a wide range of spectral types, including early type O, B,

and A stars. These were unexpected, at least in terms of acoustic heating models, because these stars were not thought to have surface convection zones.

P/OF should contribute to the development of the study of stellar coronae in many of the ways in which it will contribute to solar coronal physics. The energy band is the right one for detecting the nonthermal and high-temperature components. It is ideal for measuring the temperatures of coronae and monitoring for hard X-ray stellar flares. It is even conceivable that the RS CVn systems will provide extended hard X-ray sources that can be imaged. The Solid State Spectrometer on Einstein has shown that the spectra of these systems can usually be resolved into a low- and a high-temperature component. The low temperature component is associated with the optically active K star in the binary system and disappears when that star is eclipsed. The high-temperature component is more extended (not eclipsed), and the indications are that it occupies a volume comparable to the orbital separation of the system. In Capella, which represents the favorable case of wide separation in a nearby system, this component will extend for ~ 0.2 arc sec, if its size is on the order of the orbital major axis.

The X-ray astronomy of stellar coronae has just begun to develop into a rich field with HEAO-1 and the Einstein Observatory. It promises to advance dramatically when new facilities such as P/OF become available.

5.7 Cosmic X-ray Observational Requirements

The scientific program described in the earlier parts of this chapter can be achieved using the CAI and FT X-ray imaging instruments in the Model Payload. Instrumental characteristics required for X-ray astronomy applications do not differ greatly from those given in section 2.6 for the solar observations.

One main reason why this is the case is that typical observations in both categories require detection of *roughly the same fluence per pixel, over very similar energy ranges.* A bright solar flare will provide on the order of 10^4 cts/(cm^2 sec) at 5 keV and 10^2 – 10^3 cts/(cm^2 sec) at 20 keV. Solar scientific objectives call for these fluxes to be used to produce images with pixel sizes of ~ 0.2 arc sec and time resolution of ~ 5s. This corresponds to a signal of 10^{-1} to 10^{-2} cts/(cm^2 pixel), if one considers that it is necessary to follow the evolution of the flare down to fluxes at least an order of

magnitude below the peak value. For comparison, a 0.03 μJy source (at 5 keV) integrated for 10^4 s also gives a fluence per pixel of $\sim 10^{-1}$ cts/(cm^2 pixel). The steepness of solar spectra, the short integration time and the large number of pixels in the solar flare image all contribute to the coincidence in the two numbers.

Bearing in mind that the requirements overlap for the most part, we discuss here a few of the differences between the solar and astronomical needs.

a) *Response to hard X-rays.* For astronomical purposes it is important for P/OF to cover the high-energy range of AXAF, 5—10 keV. Good performance near the Fe lines (7 keV) is important. Measurement of hard spectral components in AGNs, binary pulsars, and other sources requires good response up to $\sim$ 100 keV.

b) *Spatial Resolution.* Because of the small angular size of many of the sources, angular resolution better than 1 arc sec is frequently needed.

c) *High Sensitivity.* Many of the observations described concern faint sources. Just as with the solar observations, there will be many important astronomical goals requiring the full sensitivity of the instrument.

d) *High Time Resolution.* For some X-ray astronomy purposes (e.g., observation of fast pulsars) one would like time resolution below 0.1 s; occasionally it would be useful to have 1 ms timing resolution (for example, in order to image the Crab Nebula by selecting times when the Crab Pulsar is turned off).

e) *Broad Spectral Range.* Response to X-rays below 5 keV will be important especially when observing variability characteristics of bright sources; response down to 2 keV would be sufficient for the purposes described in this chapter.

f) *Broad Field of View.* Surveys and imaging of extended sources would frequently make use of a 1° field of view.

g) *Long Observing Interval.* Long intervals are needed both for integration time on faint sources and to study temporal variability in the brighter sources.

In converting these requirements into design approaches, the recommendations made in section 2.7

generally cover the cosmic X-ray needs as well. The possible differences to note are (i) the occasional need for finer timing resolution, (ii) a far *less* stringent need to protect against strong fluxes of soft X-rays and (iii) the desirability of reaching energies as low as 2 keV.

Acton, L.W., Canfield, R.C., Gunkler, T.A., Hudson, H.S., Kiplinger, A.L., Leibacher, J.W., 1982, **Ap. J., 263,**

Allen, C.W., 1963, **Astrophysical Quantities** (London: Athlone Press).

Anderson, K.A., and Winckler, J.R., 1962, **J.G.R., 67,** 4103.

Antonucci, E., and 8 co-authors, 1982, **Solar Phys., 78,** 107.

Bai, T., 1982, in R.E. Lingenfelter, H.S. Hudson, and D.M. Worrall (eds.), **Gamma Ray Transients and Related Astrophysical Phenomena,** (New York: A.I.P.), p. 409.

Bai, T., Hudson, H.S., Pelling, R.M., Lin, R.P., Schwartz, R.A., and von Rosenvinge, T.T., 1982, **Ap. J.,** to be published (UCSD SP 82-20).

Becker, R.H., Helfand, D.J., and Szymkowiak, A.E., 1982, **Ap. J., 255,** 557.

Bradt, H., Garmire, G., Oda, M., Spada, G., Sreekantan, B., and Gorenstein, P., 1968, **Space Sci. Rev., 8,** 471.

Branduardi, G., Kylafis, N.D., Lamb, D.Q., and Mason, K.O., 1980, **Ap. J., 235,** L153.

Brown, J.C., Melrose, D.B., and Spicer, D.S., 1979, **Ap. J., 228,** 592.

Brueckner, G., 1974, in G. Newkirk, Jr. (ed.), **IAU Symposium #57,** (Dordrecht: Reidel), p. 333.

Brueckner, G., 1980, in P.A. Wayman (ed.) **Highlights of Astronomy, 5,** 557.

Carrington, R.C., 1859, **M.N.R.A.S., 23,** 131.

Cheng, C.-C., and 7 co-authors, 1982, **Ap. J. (Lett.), 253,** 367.

Chupp, E.L., 1981, in R.E. Lingenfelter, H.S. Hudson, and D.M. Worrall (eds.), **Gamma Ray Transients and Related Astrophysical Phenomena,** (New York: A.I.P.), p. 363.

Dere, K.P., 1982, **Solar Phys., 75,** 189.

Dicke, R.H., 1968, **Ap. J. (Lett.), 153,** L101.

Donnelly, R.H., and Kane, S.R., 1978, **Ap. J., 222,** 1043.

Duijveman, A., et al., 1982, **Solar Phys.,**

Duncan, M.J., and Wheeler, J.C., 1980, **Ap. J. (Lett.), 237,** L27.

Eaton, J.A., and Hall, D.S., 1979, **Ap. J., 227,** 907.

Fabian, A.C., Willingale, R., Pye, J.P., Murray, S.S., and Fabbiano, G., 1980, **M.N.R.A.S., 193,** 175.

Feigelson, E.D., Schreier, E.J., Delvaille, J.P., Giacconi, R., Grindlay, J.E., and Lightman, A.P., 1982, **Ap. J., 251,** 31.

Feldman, U., et al., 1981, **J.G.R., 86,** 5408.

Fenimore, E.E., and Cannon, T.M., 1978, **Appl. Optics, 17,** 337.

Fenimore, E.E., Cannon, T.M., van Hulsteyn, D.B. and Lee, P., 1979, **Appl. Optics, 18,** 945.

Fomalont, E.B., and Wright, M.C.H., 1974, in G.L. Verschuur and K.I. Kellerman (eds.), **Galactic and Extragalactic Radio Astronomy** (New York: Springer), 256.

Frost, K.J., and Dennis, B.R., 1971, **Ap. J., 165,** 655.

Gardner, B.M., and 7 co-authors, 1981, **Bull. A.A.S., 13,** 903.

Giacconi, R., and 30 co-authors, 1979, **Ap. J., 230,** 540.

Goldreich, P., and Julian, W.H., 1969, **Ap. J., 157,** 869.

Heise, A.C., Brinkman, J., Schrijver, J., Mewe, R., Gronenschild, E., and den Boggende, A., 1975, **Ap. J. (Lett.), 202,** L73.

Hollweg, J.V., 1978, **Rev. Geophys. Sp. Phys., 16,** 689.

Hollweg, J.V., 1981, in F.Q. Orrall (ed.), **Solar Active Regions,** (Boulder: Colorado Assoc. Univ. Press), p. 277.

Holzer, T., 1979, in D.J. Williams (ed.), **Physics of Solar Planetary Environments (Boulder, 1976),** (A.G.U.), p. 366.

Hoyng, P., and 23 co-authors, 1981a, **Ap. J. (Lett.), 244,** L153.

Hoyng, P., and 11 co-authors, 1981b, **Ap. J. (Lett.), 246,** L155.

Hudson, H.S., 1978, **Ap. J., 224,** 235.

Hudson, H.S., Lin, R.P., and Stewart, R.T., 1981, **Solar Phys., 75,** 245.

Hurford, G.J., 1982, private communication.

Hurford, G.J., and Hudson, H.S., 1979, (BBSO#0180), (UCSD-SP-79-27) to be submitted to **Astron. Astrophys.** (1982).

Hundhausen, A.J., 1972, **Coronal Expansion in the Solar Wind**, (New York: Springer).

Jacques, S.J., 1977, **Ap. J., 215**, 942.

Kahler, S., 1972, **Solar Phys., 25**, 435.

Kahler, S.W., Hildner, E., and van Hollebeke, M.A.I., 1978, **Solar Phys., 57**, 429.

Kahler, S.W., and 30 co-authors, 1982, **Ap. J., 252**, 239.

Kane, S.R., 1972, **Solar Phys., 27**, 174.

Kane, S.R., and 10 co-authors, 1980, in P.A. Sturrock (ed.), **Solar Flares**, p. 187.

Kane, S.R., and Donnelly, R.H., 1971, **Ap. J., 164**, 151.

Kane, S.R., and Raoult, A., 1981, **Ap. J. (Lett.), 248**, L77.

Kane, S.R., Fenimore, E.E., Klebesadel, R.W., and Laros, J.G., 1982, **Ap. J. (Lett.), 254**, L53.

Klein, L., Anderson, K., Pick, M., Trottet, G., Vilmer, N. and Kane, S., 1982, **Solar Phys.**, to be published.

Kohl, J.L., and 7 co-authors, 1980, **Ap. J. (Lett.), 241**, L117.

Kohl, J.L., Withbroe, G.L., Weiser, H., MacQueen, R.M., and Munro, R.H., 1981, **Sp. Sci. Rev. 29**, 419.

Kohl, J.L. and Withbroe, G.L., 1982, **Ap. J., 256**, 263.

Kopp, R.A., and Pneuman, G.W., 1976, **Solar Phys., 50**, 179.

Kundu, M.R., 1965, **Solar Radio Astronomy**, (Interscience, New York).

Kundu, M.R., Gergely, T.E. and Kane, S.R., 1982, **Solar Phys., 79**, 107.

Kylafis, N.D., and Lamb, D.Q., 1979, **Ap. J. (Lett.), 228**, L105.

Lamb, F., and Pines, D. (Eds.), 1979, **Compact Galactic X-ray Sources** (Physics Department, University of Illinois).

Lantos, P., Kerdraon, A., Rapley, C.G., and Bentley, R.D., 1981, **Astron. Astrophys., 101**, 33.

Lea, S.M., and 6 co-authors, 1981, **Ap. J., 246**, 369.

Leventhal, M., MacCallum, G.J. and Stang, P.O., 1978, **Ap. J., 225**, L11.

Lin, R.P., 1974, **Space Sci. Revs., 16**, 189.

Lin, R.P., and Hudson, H.S., 1971, **Solar Phys., 17**, 412.

Lin, R.P., and Hudson, H.S., 1976, **Solar Phys., 50**, 153.

Lin, R.P., Evans, L.G. and Fainberg, J., 1973, **Astrophys. Letters, 14**, 191.

Lin, R.P., Schwartz, R.A., Pelling, R.M., and Hurley, K.C., 1981, **Ap. J. (Lett.), 251**, L109.

Makishima, K., and Pelling, M., 1982, private communication.

Makishima, K., and 6 co-authors, 1978, in van der Hucht, K., and Vaiana, G.S. (eds.), **New Instrumentation for Space Astronomy** (New York: Pergamon).

Marsh, K.A. and Hurford, G.J., 1982, **Ann. Rev. Astron. Astrophy., 20**, 497.

Matilsky, T., Shrader, C. and Tananbaum, H., 1982, **Ap. J. (Lett.), 258**, L1.

Matteson, J.L., 1982, in G.R. Riegler and R.D. Blandford (eds.), **The Galactic Center** (New York: AIP), p. 109.

Motch, C., Ilovaisky, S.A., and Chevalier, C., 1982, submitted to **Astron. Astrophys.**

Murray, S.S., Fabbiano, G., Fabian, A.C., Epstein, A., and Giacconi, R., 1979, **Ap. J. (Lett.), 234**, L69.

Nolan, P.L., and 8 co-authors, 1981, **Ap. J., 246**, 494.

Oda, M., 1965, **Appl. Opt., 4**, 143.

Oda, M., and 6 co-authors, 1971, **Ap. J. (Lett.), 166**, L1.

Oda, M., 1982, COSPAR-Ottawa, to be published in **Adv. Space Res.**

Ohki, K., and 8 co-authors, 1982, **Proc. Hinotori Symposium on Solar Flares**, p. 102.

Pneuman, G., 1982, **Solar Phys., 78**, 229.

Potter, D.W., Lin, R.P., and Anderson, K.A., 1980, **Astrophys. J. (Lett.), 236,** L97.

Proctor, R.J., Skinner, G.K., and Willmore, A.P., 1978, **M.N.R.A.S., 185,** 745.

Pye, J.P., Pounds, K.A., Rolf, D.P., Seward, F.D., Smith, A., and Willingale, R., 1981, **M.N.R.A.S., 194,** 569.

Ramaty, R., and 11 co-authors, 1980, in P. Sturrock (ed.), **Solar Flares,** (Boulder: Colorado Assoc. Univ. Press), p. 117.

Reichert, G., 1982, Ph.D. Dissertation, University of California, Berkeley (unpublished).

Robinson, R.D., and Smerd, S.F., 1975, **Proc. Ast. Soc. Australia, 2,** 374.

Rosner, R., 1982, **Advances in Space Research** (to be published).

Rothschild, R., and 8 co-authors, 1981, **Space Science Instrumentation, 4,** 269.

Rothschild, R.E., Boldt, E.A., Holt, S.S., and Serlemitsos, P.J., 1974, **Ap. J. (Lett.) 189,** L13.

Sahal-Brechot, S., 1974, **Astron. Astrophys., 36,** 355.

Sargent, W.L.W., Young, P.J., Boksenberg, A., Shortridge, K., Lynds, C.R., and Hatwick, F.D.A., 1978, **Ap. J., 221,** 731.

Seward, F., Grindlay, J., Seaquist, E., and Gilmore, W., 1981, **Nature, 287,** 806.

Sheeley, Jr., N.R., and 12 co-authors, 1975, **Solar Phys., 45,** 377.

Skinner, G.K., 1979, **Proc. Roy. Soc. London A, 366,** 345.

Smith, D.F., 1974, **Space Sci. Rev., 16,** 91.

Snyder, W.A., and 12 co-authors, 1980, **Ap. J. (Lett.), 237,** L11.

Sturrock, P.A. (ed.), 1980, **Solar Flares,** (Boulder: Colorado Associated University Press).

Svestka, Z., 1976, **Solar Flares,** (Dordrecht: D. Reidel).

Svestka, Z., and 14 co-authors, 1982a, **Solar Phys., 75,** 305.

Svestka, Z., and 6 co-authors, 1982b, **Solar Phys., 78,** 271.

Tanaka, K., Watanabe, T., Nishi, K., and Akita, K., 1982, **Ap. J. (Lett.), 254,** L59.

Tennant, A.F., Mushotzky, R.F., Boldt, E.A., and Serlemitsos, P.J., 1981, **Ap. J., 251,** 15.

Trumper, J., Pietsch, W., Reppin, C., Sacco, B., Kendziorra, E., and Staubert, R., 1977, **Ann. N.Y. Acad. Sci., 302,** 538.

Tsuneta, S., and 9 co-authors, paper presented at U.S.-Japan Seminar on Solar Flares, Tokyo, October, 1982.

van Beek, H.F., Hoyng, P., Lafleur, B. and Simnett, G.M., 1980, **Solar Phys., 65,** 39.

Watson, M.G., Willingale, R., Grindlay, J.E., and Hertz, P., 1981, **Ap. J., 250,** 142.

Webb, D.F., and 6 co-authors, 1980, in P. Sturrock (ed.), **Solar Flares,** (Boulder: Colorado Assoc. Univ. Press), p. 471.

Webb, D.F., and Kundu, M.R., 1978, **Solar Phys., 57,** 154.

Wild, J.P., Smerd, S.F., and Weiss, A.A., 1963, **Ann. Revs. Astron. Astrophys., 1,** 291.

Withbroe, G.L., Kohl, J.L., Weiser, H., and Munro, R.H., 1982, submitted to **Space Sci. Rev.**

Wolff, R.S., and Novick, R., 1976, **Astrophys. Letters, 18,** 29.

Young, P.J., Westphal, J.A., Kristian, J., Wilson, C.P., and Landauer, F.P., 1978, **Ap. J., 221,** 721.

Zirker, J.B. (ed.) 1977, **Coronal Holes and High Speed Wind Streams,** (Colorado Assoc. Univ. Press).

1. REPORT NO. NASA TP-2168	2. GOVERNMENT ACCESSION NO.	3. RECIPIENT'S CATALOG NO.
4. TITLE AND SUBTITLE The Pinhole/Occulter Facility		5. REPORT DATE April 1983
		6. PERFORMING ORGANIZATION CODE
7. AUTHOR(S) Edited by E. A. Tandberg-Hanssen, H. S. Hudson*, J. R. Dabbs, and W. A. Baity *		8. PERFORMING ORGANIZATION REPORT #
9. PERFORMING ORGANIZATION NAME AND ADDRESS George C. Marshall Space Flight Center Marshall Space Flight Center, Alabama 35812		10. WORK UNIT NO. M-409
		11. CONTRACT OR GRANT NO.
		13. TYPE OF REPORT & PERIOD COVERED
12. SPONSORING AGENCY NAME AND ADDRESS National Aeronautics and Space Administration Washington, D.C. 20546		Technical Paper
		14. SPONSORING AGENCY CODE

15. SUPPLEMENTARY NOTES

*Dr. Hudson and Dr. Baity are associated with the University of California, San Diego.

16. ABSTRACT

The outer solar atmosphere exhibits a great variety of dynamic and energetic plasma phenomena, from the catastrophic energy release of solar flares to the steady acceleration of the solar wind. Observations from space in the past two maxima of the solar activity cycle have more than whetted the appetite for understanding the physics of the solar corona. The Pinhole/Occulter Facility contains the instruments necessary for achieving fuller knowledge: broad-band X-ray imaging, combined with simultaneous ultraviolet and white-light spectroscopy and imaging.

X-ray astronomy has progressed, through the surveys by small satellites and the "deep" observations of soft X-rays by the Einstein Observatory, to a level at which it has become a major component of astronomical investigation. The Pinhole/Occulter represents the first serious effort to broaden the spectral band available to X-ray astronomers at high angular resolution (below one arc second), and it is thus an effective complement to AXAF and other future soft X-ray facilities.

17. KEY WORDS Coronagraph X-ray imaging Solar physics Solar astronomy High energy astronomy X-ray astronomy	18. DISTRIBUTION STATEMENT Unclassified – Unlimited Subject Category 92

19. SECURITY CLASSIF. (of this report) Unclassified	20. SECURITY CLASSIF. (of this page) Unclassified	21. NO. OF PAGES 52	22. PRICE A04

National Aeronautics and
Space Administration

Washington, D.C.
20546

THIRD-CLASS BULK RATE

U.S.MAIL

NASA